Title: Mind the blank: behavioral, experiential, and physiological signatures of absent-mindedness

Authors: Esteban Munoz-Musat[1,2], Arthur Le Coz[1,5], Andrew W. Corcoran[3], Laouen Belloli[1], Lionel Naccache[1,4], Thomas Andrillon[1,3,5*]

Affiliations:

[1] Sorbonne Université, Institut du Cerveau - Paris Brain Institute - ICM, Inserm, CNRS, APHP, Hôpital de la Pitié Salpêtrière, Paris, France
[2] Université Paris-Cité/Service de Neurologie Cognitive, hôpital Lariboisière-Fernand Widal. IHU reConnect, Paris, France.
[3] Monash Centre for Consciousness and Contemplative Studies, Faculty of Arts, Monash University, Melbourne, Australia
[4] Service de Neurophysiologie, Hôpital Pitié Salpêtrière, Paris, France
[5] Service des Pathologies du Sommeil, Hôpital Pitié Salpêtrière, Paris, France

*Corresponding author. Email: thomas.andrillon@icm-institute.org.

ABSTRACT:

Does being awake necessarily mean being conscious of something? This study investigates the phenomenon of Mind Blanking (MB), characterized by an "emptiness of mind", comparing it with Mind Wandering (MW) and On-task (ON) states. Using a sustained attention task and electroencephalogram monitoring, behavioral and neurophysiological signatures of MB were examined in 62 participants. MB exhibited a specific pattern of behavioral lapses, as well as decreased fast oscillatory activity and complexity over posterior electrodes compared to MW. Functional connectivity analyses revealed decreased long-range inter-areal connectivity during MB, compared to both ON and MW states. Event-related potentials with source reconstruction and temporal decoding techniques indicated a significant disruption in visual processing during MB, starting from 200 ms post stimulus and echoing into the late-stage of visual processing, suggesting a disruption of conscious access to sensory information during MB. EEG-based neural features enabled trial-level prediction of mental states, furnishing estimates of the fine-grained dynamics of consciousness beyond subjective reports. Overall, these findings challenge the notion of the wakeful conscious mind as inherently content-oriented, suggesting that MB reflects genuine gaps in the stream of conscious thoughts, arising from disruptions in the generation or accessibility of thought content

SIGNIFICANCE STATEMENT:

Employing cutting-edge neurophysiological techniques on high-density electroencephalographic recordings, our study unveils unique neurophysiological markers of mind blanking, a phenomenon characterized by lapses in conscious content amidst the flow of wakeful consciousness. Distinguished from content-oriented states such as on-task and mind-wandering, mind blanking appears to be a distinct mental state. Furthermore, we demonstrate the feasibility of decoding consciousness dynamics solely from EEG features, transcending the limitations of intermittent subjective reports. Our findings thus not only provide a novel framework for investigating the stream of consciousness but also challenge the conventional notion that wakefulness invariably signifies being conscious of something.

Keywords: Mind Blanking, Mind Wandering, EEG, Neurophysiology, Consciousness, Attention.

INTRODUCTION

> *"Consciousness, then, does not appear to itself chopped up in bits. Such words as 'chain' or 'train' do not describe it fitly as it presents itself in the first instance. It is nothing jointed; it flows. A 'river' or a 'stream' are the metaphors by which it is most naturally described. In talking of it hereafter let us call it the stream of thought, of consciousness, or of subjective life"* (William James, 1890).

In the former quote, William James pointed to two very intuitive aspects of our conscious experience[1]. First, consciousness seems *continuous* during wakefulness, without any "pauses" or breaks in the flow of contents of experience. Second, our conscious experience is dynamic and the origin of conscious content changes very frequently. Indeed, the stream of experiences can quickly shift between different external sources of information, but also turn inward towards internally generated task-unrelated thoughts, a phenomenon usually referred to as mind wandering (MW)[2,3]. Extensive research has shown that, in the brain, the transitions between task-related focus and MW involve modulations of activity of the Default-mode network (DMN)[4] as well as changes in cortical dynamics with modulations of alpha activity[5,6] and increases in slower rhythms[7]. MW research has also investigated the distinctions between different MW subtypes, stressing the importance of considering the meta-awareness or voluntariness dimensions of MW[8].

More recently, a third "mind state" has been described, challenging the idea of a continuous stream of conscious contents during wakefulness: the state of mind blanking (MB). MB is described as a waking state that is either spontaneous or intentional, during which a subject does not report any mental content, but rather the feeling of an empty mind[9]. Previous studies have shown that MB is reported about 14-18% of times during focused tasks[9,10] and about 6% of times during resting[11]. Furthermore, MB has been associated with a specific behavioral signature, distinct from both MW and task-focused states[7]. The exact nature of mind blanking is still a matter of debate[12,13] and only a few studies have attempted to investigate its neural correlates[14]. Some have reported a widespread deactivation of thalamic and cortical brain regions during spontaneous MB[15] and a more focal deactivation of the superior and inferior frontal gyri and hippocampus during intentional MB, whereas anterior cingulate cortex activation seemed to increase[16]. Others have reported an increase of functional connectivity, as measured by phase coherence metrics, during MB[17]. Finally, MB has been linked to the occurrence of sleep-like slow waves in scalp EEG[7].

Two pressing questions regarding MB remain. First, it remains unclear whether MW and MB correspond indeed to different subjective and neurophysiological states[18,19] or if they can be traced back to common underlying physiological causes expressed in varying degrees[20]. Recent evidence suggests that both MW and MB could be explained by local sleep phenomena in the brain, but with different regional distributions[7]. Other accounts suggest that MB could arise from a specific pattern of neural (de)activations or functional connectivity, distinguishable from both task-focused and MW states[15,17]. To better understand the true nature of MB in respect to both task-focused and MW states, the neural distinctions of these mind states, if any, need to be further investigated[21,22].

Second, the place of MB in the hierarchy of consciousness states needs to be clarified. Traditionally, a clear distinction was made between states of unconsciousness (e.g., coma, deep N3 sleep) and states of consciousness (e.g., normal Wakefulness, REM sleep). States of consciousness (i.e., being conscious) classically imply the existence of conscious contents (i.e., being conscious of something) whereas states of unconsciousness imply the absence of such contents. Recent work suggests that the frontier between conscious and unconscious states is not as clear-cut. Indeed, conscious experiences (dreams) are often reported during consolidated non-REM sleep[23,24]; and transient behavioral as well as electrophysiological signs of conscious processing have been recently reported during sleep including N3 sleep[25–27]. These results suggest an intriguing possibility: could the reverse phenomenon - transient absence of conscious content during wakefulness- exist[21]? If so, could MB be a potential candidate for such a particular state?

Some theoretical accounts of consciousness align with the possibility of gaps in the stream of conscious contents. For example, the Global Neuronal Workspace Theory of Consciousness (GNWT)[28,29] suggests that conscious access (and hence, reportability) to a given representation depends on the late, sustained and global 'ignition' of fronto-parietal associative areas. According to this view, consciousness is a discrete phenomenon, and windows of unconsciousness during Wakefulness could result from a gap between two ignitions. The Integration Information Theory (IIT) posits that consciousness would dissolve whenever the brain's capacity to integrate information breaks down[30]. Changes in cortical dynamics towards less integration may correspond to gaps in the stream of consciousness, much like the mirror phenomenon, local activations within sleep, is linked to dreaming[24]. The parallel with sleep and dreaming research is particularly inspiring, since extensive research has shown that (macro) unconscious states (N3 sleep, deep anesthesia, coma, the vegetative state) are characterized by : i) a decrease in neural complexity and fast neural oscillations[31–34]; ii) a breakdown of information sharing between distant cortical areas[35–38], particularly in the

delta and theta frequency bands[39,40] ; iii) impaired neural responses and representations to external stimuli, particularly during the late-stage of information processing (>300ms post-stimulus)[33,41–45]. These previous research provide candidate EEG markers to explore the signature of MB.

Here, we present compelling evidence that MB is a separate mental state, distinct from MW and task-focused states at the phenomenological, behavioral and neurophysiological levels. To provide an exhaustive characterization of the neurophysiological fingerprint of MB, we relied on previous work exploring consciousness states and contents[46]. In particular we capitalized on the use of markers tracking both background neural dynamics (complexity, information sharing) and the processing of external information (ERPs, temporal decoding) in the sensor and source space. Based on these signatures, we argue that MB could represent a failure of conscious access mechanisms, resulting in a genuine gap in the stream of conscious contents.

RESULTS

Different behavioral signatures between Mind Blanking and Mind Wandering

In these two studies, 62 healthy participants performed a modified sustained attention to response task (SART), with digits and faces as stimuli presented in separate blocks, while high-density electro-encephalogram (hdEEG) was recorded continuously. After each stimulus presentation, participants had to press a button (Go trials), or refrain from doing so whenever a “3” or a smiling face was presented (No Go trials; 1 out of 9). Stimulus onset asynchrony (SOA) varied randomly (from 750-1250ms) with a null inter-stimulus interval, and participants’ mental state was probed at random intervals (every 40-70s, uniform random jitter). Participants were instructed to report their attentional focus ‘just before the interruption’ by selecting one of four options: (1) ‘task-focused’ (ON), (2) ‘off-task’ (mind-wandering, MW), (3) ‘mind-blanking’ (MB), or (4) ‘don't remember’. Since the fourth option accounted for only 2.6% of all probes (i.e., less than two probes per participant on average) and given that previous studies did not consistently distinguish between these options[47], we merged third and fourth options as MB in all analyses (Figure 1A-B).

Participants performed this task with a high accuracy (mean accuracy of 86.5 ± 0.5% (SEM)) and with a relatively low rate of Misses (i.e., errors in Go trials, 10.4 ± 0.5%). Errors in No Go trials (False alarms [FA]) were frequent (36.7 ± 1.5%). At the subjective level, participants reported being focused on the task (ON) in only 52 ± 2.7% of the probes and otherwise reported MW (35 ± 2.3%) or MB (16 ± 1.8%) (Figure 1C). The distribution of the ON, MW and MB mind-states was not uniform across participants (see Figure 1C), with large inter-individual differences: in particular 9 participants (14.5%) did not report any MB experience.

In order to detect fine-grained modulations of behavioral performance according to the participant’s mind-state, we labeled all trials presented up to 5 seconds before each probe as corresponding to the probed state (e.g., after an ‘ON’ response, all previous trials that occurred during the previous 5 seconds were labeled as ‘ON’ trials). As previously reported in a smaller subgroup of participants (40% of the present cohort)[7], we found a significant main effect of *mind-state* on FA, misses and RTs (see Table S1). Crucially, pairwise comparisons between mind-states revealed different behavioral profiles for MW and MB: while both were characterized by more FA and misses than during ON, FA were equally frequent during MW and MB (with a non-significant trend for more FA during MW trials) and misses were more frequent during MB (i.e. MB>MW>ON) (see Table S1 and Figure 1D). Response times (RTs) were *slower* for MB (compared to both ON and MW), and *faster* for MW (compared to MB and

ON; significant difference for MW vs MB and statistical trend (FDR corrected p-value 0.1) for MW vs ON) (see Table S1 and figure 1D). In sum, while MW seemed characterized by an "impulsive profile" (more FA and faster RTs), MB presented with an "absent profile" (more misses and slower RTs), which confirms our previous findings obtained in one of the two datasets.

'Front-Back' dissociation between Mind Blanking and Mind Wandering

We next investigated neurophysiological correlates of the mind-states (ON, MW and MB) from EEG recorded during the 5s preceding each probe onset. We computed three classes of neural markers: 1) spectral markers (normalized power spectral densities (PSD) in the delta, theta, alpha, beta and gamma bands); 2) complexity markers[33,48] (Kolmogorov Complexity (KC) and Sample Entropy (SE)) and 3) connectivity markers *(weighted symbolic mutual information*[39] (wSMI) in the delta, theta and alpha bands). These markers (and other similar measures) have been previously shown to track modifications of cognitive and consciousness state in a large range of conditions, including disorders of consciousness (DoC)[33,39,49], sleep[40,50,51], hypnosis[52] and meditation[53].

All studied neural markers were modulated by the participants' mind-state. A significant main effect of *mind-state* and of *electrode location* was found for the wSMI in the delta and theta frequency bands, and a significant effect of these two main factors and their interaction was found for all other markers (linear mixed models with mind-state, electrode location and their interaction as main factors; subject ID and dataset (see Methods) were introduced as random intercepts) (see Table S2).

Spectral and complexity measures revealed different profiles for MW and MB: compared to ON, MW was associated with both an increase in fast oscillatory activity and complexity over central electrodes, and with a decrease of these metrics over fronto-polar and posterior electrodes. As for MB, compared to ON, it was associated with an increase in fast oscillatory activity and complexity over frontal and fronto-central electrodes, and with a decrease in these metrics over centro-posterior and posterior electrodes. The direct contrast between MB and MW revealed a front vs. back dissociation: while frontal and fronto-central electrodes showed faster oscillatory activity and higher complexity in MB than in MW, centro-posterior and posterior electrodes showed an opposite difference (see Figure 2A,C).

Mind-state can be modulated by arousal, with MW and MB frequency increasing in moments of hypovigilance[7,54]. Therefore, some of the observed changes in neural markers could be

explained by a decrease in alertness. To ensure that our results couldn't be *exclusively* explained by this arousal factor, we conducted a verification analysis, by including in our statistical model the vigilance score as a covariate (4-point scale, 1 = Extremely Sleepy, 4 = Extremely Alert), as well as the interaction between electrode location and vigilance score. The observed results for spectral and complexity measures were nearly identical to those previously presented, with the persistence of a clear front-back dissociation between MW and MB. See supplementary Figure S1A,C.

Breakdown of long-range information sharing during Mind Blanking.

Functional connectivity analyses revealed a significant modulation by *mind-state* of the wSMI metric in frequency bands of interest (delta, theta and alpha) (see Table S2). Post-hoc topographical analyses in sensor space revealed a progressive breakdown of connectivity from ON to MW, and then from MW to MB, particularly in the alpha band (see Figure 2B). As for spectral and complexity measures, the inclusion of vigilance score as a covariate in statistical models resulted in very similar results (see Figure S1B). To better characterize these connectivity modulations in function of mind state, we reconstructed the cortical sources of the EEG signal (N=68 cortical sources) at the trial level and computed the information metric wSMI (at different frequency bands) between each pair of sources (n=2278 connections). These sources were further grouped in 10 pairs (right and left) of 5 ROIs, according to the Desikan-Killiany atlas (frontal, limbic, temporal, parietal and occipital), obtaining thus 45 averaged connections between ROIs. Since previous studies reported modifications of coherence-based metrics during MB, we also computed in source space the Phase Locking Value (PLV), for comparison. The statistical analysis revealed a main effect of *mind-state* for all computed connectivity metrics (linear mixed model with mind-state, connection and their interaction as main factors; subject ID and dataset were introduced as random intercepts; see Table S3). As reported in a previous study[17], the coherence-based metric PLV showed an increase in inter-areal connectivity during MB, compared to both MW and ON states (see Figure 3, top panel). By contrast, the information-based metric wSMI showed the reverse pattern: for all computed frequency bands (delta, theta and alpha), a significant reduction in inter-areal connectivity was observed during MB, compared to both ON and MW (except for the connectivity in the delta band between right frontal and right occipital areas, which increased) (see Figure 3). This disruption of inter-areal connectivity during MB concerned mainly parietal areas, and in particular fronto-parietal connectivity.

The inclusion of the vigilance score in the statistical models led to results largely consistent with those previously presented for the PLV and the wSMI in the theta and alpha bands; for

the wSMI in the delta band, the results were more nuanced, revealing both increases and decreases of long-range connectivity during MB (see Figure S2).

As it will be discussed later, the contrast between the PLV and the wSMI results could reflect the relative implication of linear vs. non-linear interactions between cortical regions during these different mind states, non-linear interactions being best captured by the wSMI (see discussion).

As an interim conclusion, these neurophysiological findings confirmed and extended our behavioral results, by showing that MB is associated with a specific brain state distinct from MW. In addition, the significant disruption of long-range connectivity revealed by the wSMI metric during MB suggests a marked impairment of information sharing between cortical areas during this mind-state, as systematically observed during unconscious states.

Disruption of the brain processing of external stimuli during Mind Blanking

The processing of external information is very dependent upon the background brain activity and associated mind state, and foremost the state of consciousness. Previous research has shown that early and intermediate cortical processing is preserved in classically unconscious states such as non-REM sleep[44,55–59] or coma[60–62] (having a prognostic value in this last case). By contrast, late cortical processing seems to be associated with conscious states[25,41,42,44] and conscious processing of external information[63–66]. With this in mind, we decided to probe the differential neural fate of the presented visual stimuli according to the reported mind-state.

First, we conducted a single-trial multi-level analysis of event-related potentials (ERPs) in sensor space (see Methods for details and Table S4 for the results of the statistical model). Early processing of visual stimuli was extremely similar across ON, MW and MB mind-states. In particular, a similar posterior positivity peaking around 100-150 ms after stimulus presentation, and corresponding to the P1 component[67], was present in all 3 conditions (see Figure 4A). Visually, this P1 component seemed more pronounced in ON and MW states than in MB, but very few electrodes showed a significant effect (≤3). No significant differences were observed between MW and ON during the early time-window (see Figure 4B). Crucially, stimulus processing diverged massively as a function of mind-state during the late time-window (>350ms). In ON trials, a classical P3b component (central positivity) spanned roughly from 400 to 650 ms after stimulus onset. In MW trials, this P3b pattern was still observable, but with a longer latency, a reduced maximal amplitude and a shorter duration. Finally, in this late time-window, no clear P3b response was observable in MB trials; amplitudes of MB ERPs

were significantly decreased as compared to ON and MW, with only a reduced and left-lateralized response, possibly related to motor responses (Figure 4A-B). As a control, we also conducted the previously described analysis independently for each stimulus type (faces vs digits). ERP profiles show differences in the timing of early and late components yet, for digits and faces, MB trials were characterised by a disruption of late components compared to ON trials (see Figure S3).

While univariate methods such as ERPs provide with important information about the amplitude and timing of cortical activations in response to external stimuli, multivariate decoding methods allow for a more subtle analysis, and provide information at the level of neural representations. We wanted to answer the following question: does brain activity encode relevant information about the presented stimuli, and how these neural representations vary as a function of the reported mind-state? To do so, we tested whether we could decode stimulus type (Faces vs. Digits) from brain responses using multivariate pattern analysis (MPVA), with the Temporal Decoding method[43,68]. Briefly, this type of analysis consists in using a subset of the data to train a linear classifier at each time-point to differentiate trials where a *Face* was presented from trials where a *Digit* was presented, and then testing its performance, independently at each time-point, in a different subset of the data. We ensured a comparable number of trials between mind-states by randomly subsampling trials from each mind-state. Then, we applied the Temporal Decoding method independently for each mind state, and statistically compared the obtained performance scores (ROC AUC) with a dummy random distribution centered around 0.5 (chance level performance). Results can be found in Figure 4C. For ON trials, we found several time-windows with significant decoding compared to chance level performance. The first one, around 200ms, coincided with a sharp decoding peak (AUC>0.65). The other ones, spanning from 250ms to 580ms, corresponded to a sustained period of decoding. For MW trials, we found a similar initial peak around 200ms; however, later time-windows with significant decoding were sparser, with a period around 350ms, and then a few significant time-points after 400ms. Crucially, we didn't observe any statistically significant decoding for MB trials.

Given these results, we reconstructed the cortical sources of the EEG signals at trial level, and compared the post-stimulus activations (time-window: 0-700ms) to the activations during the baseline period (-250 - 0 ms). For both ON and MW trials, we observed a significant activation of bilateral occipital visual regions (around 200-300 ms post-stimulus), followed by an activation of regions along the ventral and dorsal visual streams (300-600ms), reaching some frontal areas (around 500ms post stimulus). Responses in MW trials were smaller, delayed and less spatially extended compared to ON. Importantly, for MB trials, we observed

only sparse activations, mostly left-sided (contralateral to motor responses), with no clear involvement of the dorsal or ventral visual streams (see Figure 5).

In sum, while the essential processing steps of visual information seem preserved during MW compared to ON-task, these processes appear significantly disrupted during MB, particularly the late responses usually associated with conscious access.

Trial-by-trial prediction of mind-state based on EEG neural features.

The exploration of the dynamics of consciousness is limited by the reliance on the discrete sampling of experience through mind probes and subjective reports. To circumvent this snapshot approach, we set out to predict participants' mind-states on a trial-by-trial basis using neural features. We gathered all the previously presented EEG markers from stimulus-centered epochs (-0.25 to 0.75 s relative to stimulus onset), for all trials. We then trained and cross-validated, independently for each subject, machine learning classifiers (Random Forest), using exclusively trials within the 5 seconds preceding probe onsets (since we can label these trials as "ground truth" based on subjective reports). Importantly, during the cross-validation procedure, we grouped trials by experimental block (6 blocks for each participant) to avoid overfitting due to temporal proximity between trials (see Methods for more details). In multiclass classification (ON vs MW vs MB), the median classifier's balanced accuracy score across participants was of 46%, significantly above chance level performance (median chance level (500 permutations): 37%, FDR corrected p-value=9.10^{-6}, Wilcoxon rank-sum test, see Methods for more details) (Figure 6A; Table S5 and S6). Classifiers' performances varied sharply between participants with classification scores above 60% for some participants, while for other participant's the classifier presented with chance-level performance.

We then used our trained classifiers to estimate the mind-state in non-labeled trials (>5s before probe onsets). To estimate the reliability of these single-trial predictions, we computed metrics of behavioral performance in these trials for each predicted state ($\widehat{ON}$, $\widehat{MW}$, $\widehat{MB}$). Indeed, as shown previously, ON, MW and MB have different behavioral signatures so we can use behavior to check if these signatures are consistent with our predictions. And indeed, behavioral patterns of predicted states were very similar to the corresponding labeled states: we observed more misses in (predicted) $\widehat{MB}$ trials than in $\widehat{ON}$ and $\widehat{MW}$ trials, as well as longer RTs in $\widehat{MB}$ as compared to $\widehat{MW}$ and $\widehat{ON}$ trials (see Table S7 and Figure 6B). We also observed more FA in $\widehat{MW}$ compared to $\widehat{ON}$ trials but RT were significantly slower and not faster (see

Figure 1). This pattern of results suggest that our classifiers were able to retrieve the behavioral signatures on ON, MW and MB states for unprobed trials.

DISCUSSION

Mind Blanking corresponds to a specific brain state, different from Mind Wandering

In this study replicating and extending a previously published study[7], we examined the behavioral and neural correlates of MB, compared to those of MW and ON states. During a sustained attention task, we confirmed our previous findings[7] showing that MB corresponds to a distinct mental state, characterized by a specific behavioral profile and by specific neural signatures. At a behavioral level, MB was characterized by response slowing and higher rate of misses, compatible with participants' subjective report of having been "absent minded" during those moments. This behavioral profile was different from the one observed during MW that was characterized by an acceleration of responses and more false alarms, suggestive of an 'impulsive' pattern of behavior. These differences in behavioral outcomes between MW and MB were previously reported in different tasks (e.g., reading)[69] or even task-free resting state (RT computed on probe responses)[54]. At the neural level, both state markers (spectral, complexity and connectivity measures) and brain responses to external stimuli differentiate MB from MW and ON states. This complements previous findings in fMRI associating spontaneous MB with a pattern of whole-brain hyper-connectivity and de-activation[15,17]. A multivariate combination of these neural metrics allowed for higher than chance prediction of mind-state on a trial-by-trial basis, further supporting the idea that MB, MW and ON states correspond to different mental and neurophysiological states. Taken together, these multimodal results reaffirm the specificity of MB as a distinct mental state[22].

These results face the intrinsic limitations of the validity and reliability of self-reports during experience sampling[70]. Since we used a probe-catching method where subjective reports were assessed every 1 min or so, we cannot exclude the possibility of mental contents/states happening during the interprobe intervals that participants could not report. Moreover, the experience sampling method does not allow to determine precisely the time window that corresponds to a given mind-state. As a first step towards addressing this limitation in the future, we tried to predict the participant's mind-state without reports using multivariate classifiers trained with neural metrics during those trials. Finally, our criterion for considering trials as belonging to a particular mind state (5 seconds) was motivated by technical reasons (see Methods), and not hypothesis or data-driven.

Front vs Back dissociation between Mind Blanking and Mind Wandering

We found that spectral and complexity markers display opposite topographical profiles for MW and MB: whereas MB was characterized by an increase of both complexity and fast oscillatory activity over frontal electrodes (compared to MW), it was also characterized by a decrease in these same metrics over posterior electrodes. These results are in line with previous analyses in a subset of our dataset (40% of the current data)[7], that found evidence for sleep-like slow-waves in both MW and MB, but with different regional localizations: while MW was associated with the presence of wake slow-waves over frontal scalp regions, MB was associated with their extension to posterior regions. Two previous fMRI studies showed that spontaneous MB is associated with an extensive cortical and thalamic de-activation as well as a widespread positive phase-coupling between brain regions[15,17]. Interestingly, chemogenetic inhibition of the mouse prefrontal cortex can result in (i) a decrease in neuronal firing, (ii) the presence of slow oscillations, (iii) an increase in functional connectivity[71], which suggests that the different neural correlates of MB (slow waves, deactivation and hyper-connectivity) could reflect the same neural mechanisms.

These results contrast with another study in fMRI focusing this time on *voluntary* MB, which showed its association with a deactivation of lateral prefrontal regions and hippocampus, but an activation of anterior cingulate cortex[16]. While our spectral and complexity measures were computed in sensor space, and therefore lack precise anatomical information, the observed increase in fast oscillatory activity and neural complexity over centro-anterior electrodes during MB could also be related to ACC activation. These findings are also in line with studies contrasting episodes of MW in which participants are aware or unaware of their own MW. When caught unaware, participants exhibited more activation in frontal areas (dorsal Anterior Cingulate Cortex and ventral Pre Frontal Cortex)[72], which could be related to the increase in fast oscillations we observed in MB, possibly suggesting a continuum between MB and unaware MW. Overall these results highlight the necessity to refine the phenomenological characterization of MB in order to better apprehend its neural correlates[12,13]. It further enriches the literature on spontaneous thoughts and experiences, which previously focused on MW but stressed the importance of considering phenomenal dimensions of MW such as meta-awareness, voluntariness or emotional valence. With MB, we emphasise that the continuous presence of experiential contents should not be taken for granted.

Increased phase synchrony with decreased information sharing between distant brain regions during Mind Blanking

To date, previous studies have reported mixed results regarding functional connectivity during MB. A previous study using fMRI[16] revealed lower functional connectivity between the default mode network and frontal, visual, and salience networks during voluntary MB as compared to MW. By contrast, using a coherence-based measure, a recent study[17] found a pattern of global positive connectivity during spontaneous MB. Beyond potential differences between voluntary and spontaneous MB, it is important to consider that functional connectivity results depend very much on the type of measure being computed. In the present study, we computed two different metrics: the PLV[73], a classical coherence-based measure that captures strictly linear correlations, and the wSMI, an information theory based measure which favors non-linear correlations over purely linear ones[39]. While the PLV showed an increase of inter-areal connectivity in MB as compared to both ON and MW (in line with the previously mentioned study), the wSMI revealed the inverse pattern, with reduced inter-areal (and more specifically, fronto-parietal) connectivity. Dissociations between coherence-based measures and the wSMI have already been reported, for example when contrasting Wakefulness and N3 sleep, where the whole-brain wSMI was significantly decreased in N3 sleep compared to wakefulness, whereas the wPLI (weighted Phase Lag Index) was not[74]. Our results could reflect a dissociation between increased phase-synchrony with decreased information sharing in MB, which could be caused by the occurrence of synchronous episodes of slow waves and neural silencing over associative cortices[75,76]. This model stresses the influence of episodes of hypo-arousal in the occurrence of MB but does not exclude that MB could also occur in states of hyper-arousal as suggested elsewhere[54].

Disrupted neural representations of external stimuli during MB.

Stimulus-induced activity analyses (ERPs, source reconstruction and temporal decoding) revealed similar patterns of processing of task stimuli during ON-task and MW states, significantly different from those observed during MB.

The most obvious difference between mind-states concerned the P3b component. A P3b response (central positivity between 400 and 600 ms post-stimulus) was clearly present during ON-task, was reduced but still observable during MW and seemed to lack during MB trials. While the neural correlates and signatures of the conscious processing of external information remain highly debated[77,78], previous studies[41,64,65] have proposed the P3b component as an EEG signature of conscious access. This interpretation remains debated, since some authors have claimed that the P3b relates more to post-perceptual processes associated with

(external) report than to conscious awareness *per se*[79,80]. The reduction of the P3b observed in MW (shorter duration and decreased amplitude compared to ON-task) is in line with previous findings showing the impact of top-down attention on the P3b[81]. This reduction suggests the superposition of stimulus-unrelated processes during the time-window of the P3b response during MW. This last interpretation is in agreement with a recent study[63], which demonstrated that the P3b can be modulated by participants' attentional focus but conscious perception is always associated with a P3b-like activation of a broad set of associative cortical areas (frontal, parietal and temporal) even in the absence of report. When participants were paying attention and reported on the stimuli, additional cortical areas becoming involved during the same time window lead to a full-fledged P3b. Our source localization results align with this model with a similar activation of the dorsal and ventral visual streams during the late time-window for both ON and MW conditions, reaching some frontal areas in both conditions, but with a less spatially extended response during MW. Crucially, MB showed here a very different ERP signature at the sensor and source level. The relative absence of a P3b response as well as the absence of clear activation of the ventral/dorsal visual streams strongly suggests the absence of conscious access to external visual stimuli in MB trials in contrast with both ON and MW trials.

We also observed differences at the level of early visual processing between the different mind states. While no major differences were observable in sensor-space ERPs during the early time-window (<300ms post-stimulus), our temporal decoding analysis revealed the emergence of distinct visual neural representations around 150-200ms post-stimulus for both ON and MW trials (significant decoding against chance level performance of stimulus category), while this was not the case for MB trials (despite the fact that the number of trials were balanced across conditions). The absence of a significant encoding of visual stimuli over occipital areas around 200ms could suggest a disruption of the actualization of visual representations during MB. This aligns with the pattern of global cortical deactivations reported during MB[15]. It further suggests that the lack of late potentials observed during MB could be due to a weaker or absent sensory activation, failing to ignite the cascade of activations observed in ON and MW, albeit with decreased amplitude for the latter.

Probing mind-state without external reports

The stream of conscious experiences is private and probing for its contents and dynamic is only possible with a sparse and disruptive sampling approach. We attempted here to bypass these reports by leveraging our new correlates of MW and MB. We showed first that we could predict above chance the mind-state category of trials just before a probe (using the mind-state reported following the probe as a ground truth) using a multivariate combination of

different neural markers. Second, we applied the same algorithm to predict mind-states for trials away from the probes, so during moments where we do not have participant's mind-state reports. We could retrieve the behavioral signatures of these states, which suggests that this MVPA approach partially captures a similar dynamics of conscious experience as evidenced in trials in which participants reported on their mental state. While the accuracy of our classifier approach remains very limited, this proof of concept provides an interesting new approach to estimate the second-by-second dynamics of mental states beyond the classical minute-by-minute sampling of subjective experience, paving the way for a fine-grained exploration of the dynamics of consciousness, without under-sampling or interfering with these dynamics by requiring a verbal report.

Conclusion: is Mind Blanking a state without conscious content during wakefulness?

In the introduction of this paper, we presented the predicted neural correlates of a potential contentless conscious state during wakefulness, based on theoretical[28,29,82] and empirical[25,33,39,40,63] considerations. We showed here that the state of MB, a phenomenological, behavioral and neurophysiological distinct state from MW, fulfils these predictions. First, as predicted, the sharing of information between distant cortical areas was disrupted during MB, in particular in the delta and theta frequency bands. Second, the neural representations of external stimuli were significantly disrupted during MB, starting from early periods of processing and echoing into late processing, usually associated with conscious access, with a lack of the usual signatures of conscious access during this mind-state. Finally, spectral, complexity and coherence based connectivity metrics point towards the hypothesis of neural silencing of posterior associative cortices, a key node for consciousness according to most theoretical accounts[29,83]. Since we studied MB in a specific context and task-design, it is possible that some of the markers obtained here would not generalise to other instances of MB. Yet, some of the markers evidenced in this study are compatible with those obtained using a different neuroimaging technique (fMRI) and without a task[15,17].

The presence or absence of internally generated representations during this mind-state remains an open question, and the impression of an "empty mind" reported by the participants during MB could be accounted for by different mechanisms (i.e., lack of metacognitive awareness, lack of memory encoding, language limitations) other than a lack of conscious experience altogether[13]. Still, based on the above presented results, we argue in favour of the more radical interpretation of MB as a "content-free" mind state. This would challenge our intuition of a continuous conscious content during wakefulness. In this view, conscious experience would be a discrete phenomenon, with discrete temporal islets with conscious

content, separated by brief contentless periods[82]. While puzzling, this perspective would bring even more value to those precious moments of conscious experience.

METHODS

Experimental procedure and data collection

Participants

A total of sixty-eight (N = 68) healthy adult subjects were enrolled in this study. Thirty-two (N=32) were recorded at the Monash University (Melbourne, Australia), between June 2018 and February 2019. An additional set of thirty-six (N=36) subjects were recorded at the Paris Brain Institute (Paris, France) from June 2024 to September 2024. The original experiment (Monash) was conducted in English, and instructions were translated in French for the Paris experiment. All other materials and procedures (including the EEG equipment) were similar for the two groups. Due to technical complications during the recording process or suboptimal physiological recording quality identified via retrospective visual examination of the data, six individuals were excluded from subsequent analysis. The final study group, comprising 62 participants (age: 27.9 ± 0.7 years, mean ± standard deviation (age missing for one individual); 31 females), was included in all analyses. Prior to study involvement, participants submitted written informed consent. Both sites Human Research Ethics Committees approved the study protocol (Monash University Human Research Ethics Committee, Project ID: 10994 ; and Comité d'Éthique de la Recherche (CER) de Sorbonne Université, Project ID: CER-2023-DEGRAVE-MW_Respi)

Experimental design and stimuli

Participants were positioned in a dimly lit room, seated approximately 60 cm away from a computer screen with their chin supported. Task instructions, stimuli presentation, and button response collection were executed using the Psychtoolbox extension for Matlab (Mathworks, Natick, MA, USA).

The experimental design involved two adapted SARTs, where participants were instructed to focus on a series of human face images during Face SART blocks and on digits during Digit SART blocks. The sequence of Face and Digit blocks was pseudo-randomized for each participant. Each block lasted for roughly 12-15 minutes, with rest periods permitted between blocks. Participants completed three Face SART and three Digit SART blocks, totalling a duration of 86.7 ± 1.2 minutes (mean ± standard deviation) for the SART, and 108.4 ± 3.4 minutes for the entire recording session. Prior to each type of Face and Digit SART, participants underwent a brief training session (27 trials) with performance feedback on correct trials and average reaction times (RTs). Participants were urged to prioritize accuracy over speed.

Face and digit stimuli were displayed continuously, with each stimulus shown for 750-1250 ms (uniform random jitter). Face stimuli were derived from the Radboud Face Database[84], consisting of eight neutral faces (four females, four males) and one smiling female face. Digits ranging from 1 to 9 were displayed in a fixed font size. For Face SART, participants pressed a button for all neutral faces (Go trials) and refrained from pressing the button for the smiling face (No Go trials). The face order was pseudo-randomized throughout the task (presentation order permuted every nine stimuli, without immediate repetition). For Digit SART, participants pressed a button for all digits except digit 3 (No Go trials), with the digit order pseudo-randomized similarly.

During the SART, stimulus presentation was halted at random intervals (every 40-70 s, uniform random jitter) accompanied by a sound and the word "STOP" on the screen. These interruptions allowed for the assessment of participants' mental states using a series of eight questions. Participants were notably instructed to report their attentional focus "just before the interruption" by selecting one of four options: (1) "task-focused" (ON), (2) "off-task" (mind-wandering, MW), (3) "mind-blanking" (MB), or (4) "don't remember." Since the fourth option accounted for only 2.6% of all probes (less than 2 probes per participant on average) and previous studies do not consistently distinguish between these options[47], we combined the third and fourth options as MB in all analyses. Whenever participants chose the off-task option, they were prompted to indicate the origin of their thoughts or experiences: (1) the environment (distractions), (2) the task (interferences), or (3) internally generated contents. Participants also rated their vigilance levels over the past few trials on a 4-point scale (1 = Extremely Sleepy, 4 = Extremely Alert). Each 12-15 minute SART block contained ten interruptions (30 interruptions per SART task, 60 interruptions per participant). Participants were briefed on the interruptions and question types prior to the experiment. The mental state categories (ON, MW, and MB) were explained both orally and in writing to participants.

Physiological recordings

High-density scalp EEG data were obtained utilizing an EasyCap (Monash) or actiCap Snap (Paris) with 63 active electrodes, connected to a BrainAmp system (Brain Products GmbH). A ground electrode was positioned frontally (Fpz in the 10-20 system), while electrodes were referenced online to a frontal electrode (AFz). Additional electrodes were placed above and below the left and right canthi to record ocular movements (electrooculogram, EOG). Two electrodes were placed over the deltoid muscles to capture electrocardiographic (ECG) activity. EEG, EOG, and ECG signals were sampled at a rate of 500 Hz. Eye movements and pupil size from one eye were recorded using an EyeLink 1000 system (SR Research) but not analyzed here. In the Paris dataset, participants were also equipped with a respiratory belt.

Behavioral analyses

Go trials were deemed incorrect (Miss) if no response was registered between the onset of the stimulus and the subsequent stimulus onset. In contrast, No-Go trials were classified as incorrect (false alarm; FA) if a response was detected within the same time frame. Reaction times (RTs) were calculated from the onset of stimulus presentation. Behavioral performances for each probe were computed using trials within 5 seconds from probe onset. The choice of a 5 second window allowed the inclusion of sufficient No-Go trials for analysis (in average one No-Go trial every two probes), while focusing on trials very close from probe onset and subsequent subjective reports.

EEG preprocessing and analysis

Preprocessing

The raw EEG signal was first high-pass filtered >1 Hz, using a linear-phase, zero-phase FIR (finite impulse response) filter to remove low-frequency drifts which could negatively affect the quality of the ICA fit (see below). A notch filter was then applied (stopbands: [49, 51], [99,101] Hz, FIR filter) to remove line noise. Electrodes that were visually identified as noisy throughout the recording were removed and interpolated using neighbouring electrodes. The EEG signal was then decomposed using independent component analysis (ICA), and the components containing ocular artifacts or electrocardiogram (ECG) artifacts were removed prior to signal reconstruction.

The ICA-cleaned EEG signal was then down-sampled to 250 Hz, and low-pass filtered <60 Hz. An average reference was applied to all EEG electrodes. Finally, the continuous EEG data were segmented in two different manners, so as to obtain two sets of epochs for different analyses: from -5 to 0 seconds relative to the probe onsets ("Probe epochs"), and from -0.25 to 0.75 seconds relative to the stimuli onsets ("Target epochs"). Probe epochs were labelled according to the mind state reported by the participant at probe onset. Target epochs in the 5 second period prior to the probes were labelled according to the subjective report, all other Target epochs were considered non-labelled (unknown mind state).

Sensor space analyses

Calculation of electroencephalographic markers tracking cognitive fluctuations

Previous work has shown that cognitive and consciousness state modifications can be tracked using different spectral, complexity or connectivity measures derived from the scalp or

intracranial electroencephalographic recording. By combining these markers, it is possible to distinguish conscious participants, patients in a minimal consciousness state and patients with unresponsive wakefulness syndrome[33,34,39]. These measures can also differentiate sleep stages[40,51,74] and track cognitive and consciousness modifications related to psychedelics or meditation[53]. In our study, we computed these different measures to try to describe the neural correlates of the different mind states (ON, MW and MB). We therefore computed these measures on a trial-by-trial basis on "Probe epochs" (from -5s to 0s relative to probe onsets), the 5 second time-window allowing for both a sufficient time-period for correct maker computation and for (very) close proximity to the subjective reports.

Prior to marker computation, we performed a spatial Laplacian transformation of the EEG signal (also known as Current Source Density (CSD) estimate)[85]. We applied a spherical spline surface Laplacian transformation, with 50 Legendre terms, a stiffness of the spline of value 4 and a regularization parameter (lambda 2) of 1e-5.

Spectral markers

We computed the normalized power spectral densities (PSD) in delta (1-4 Hz), theta (4-8 Hz), alpha (8-12 Hz), beta (12-30 Hz) and gamma (30-60) frequency bands, using Welch's method. The length of each Welch segment (windowed with a Hamming window) was set to be equal to the length of the FFT (fast Fourier transform) and equal to 256 samples (1024 ms). The obtained segments were then averaged, in order to obtain a single value per epoch, channel and frequency. To obtain the normalized PSDs in each frequency band of interest, we: 1) added the raw power of all the frequencies in each frequency band of interest; and 2) computed for each trial and each electrode the normalized PSD by normalizing the raw frequency band PSD by the total power of the electrode.

Complexity markers

We computed two different complexity measures: the Kolmogorov Complexity (KC) and the Sample Entropy (SE). Although they differ in their method of calculation, both measure the level of predictability and regularity of the EEG signal: the more the signal is unpredictable, the more it's algorithmic complexity is important (more information is needed to describe the signal), and the more the complexity of the local neural processing captured by the EEG sensor is assumed to be important.

We computed these two complexity measures for each trial and each EEG electrode (n= 64). See Supplementary material of Sitt et. al (2014)[33] for a detailed description of KC, as well as

its computation. Details regarding the SE measure can be found in Richman & Moorman (2000)[48].

Connectivity markers

Weighted symbolic mutual information

We focused on the *weighted symbolic mutual information* (wSMI), a functional connectivity measure capturing linear and non-linear coupling between sensors, which relies on the symbolic transformation of the EEG signal. The wSMI assesses the degree to which two EEG sensors exhibit non-random joint fluctuations, implying information sharing. The time series X and Y in all EEG channels are initially converted into discrete symbol sequences (X^, Y^). These symbols are encoded based on the trends in amplitudes in a predetermined number of consecutive time points. The symbols are therefore defined by two parameters: the number of time points considered (k) and the temporal separation between the time points that constitute a symbol ($\boldsymbol{\tau}$). Following previous work, we chose the parameter k to be 3, implying that the symbols are constituted of three elements, leading to 3! = 6 different potential symbols in total. The parameter $\boldsymbol{\tau}$ sets the broad frequency-specific window of sensitivity of this connectivity measure, allowing to compute the wSMI in the delta ($\boldsymbol{\tau}$= 64ms), theta ($\boldsymbol{\tau}$= 32ms) and alpha ($\boldsymbol{\tau}$= 16ms) bands. For each frequency band, the joint probability of each pair of symbols co-occurring in two different time series is computed to estimate the *symbolic mutual information* (SMI) shared across two signals. To minimise volume conduction, the *weighted* symbolic mutual information disregards co-occurrences of identical or opposite-sign signals.

The wSMI between two EEG sensors is computed, after symbolic transformation, according to the following formula:

$$\mathrm{wSMI}(\widehat{X},\widehat{Y}) = \frac{1}{log(k!)} \sum_{\widehat{x}\epsilon\widehat{X}} \sum_{\hat{y}\epsilon\widehat{Y}} w(\widehat{x},\hat{y}) p(\widehat{x},\hat{y}) log \frac{p(\widehat{x},\hat{y})}{p(\widehat{x})p(\hat{y})}$$

where w(x,y) is the weight matrix and p(x,y) is the joint probability of co-occurrence of symbol x in signal X and symbol y in signal Y. Finally p(x) and p(y) are the probabilities of those symbols in each signal.

We computed, in each frequency band, and for each trial, the wSMI between each pair of electrodes (N pairs=2016). To obtain the topographical maps shown in Supplementary Figure S1, we computed, for each sensor, its median connectivity with all other sensors, obtaining a single value per channel per trial.

Phase Locking Value (PLV)

We also computed a more classical spectral connectivity measure, the Phase Locking Value (PLV), on a trial-by-trial basis. For each channel i, we extracted the instantaneous phase $\phi i^a(t)$ of the analytical signal $xi^a(t)$ of the time series $xi\,(t)$. Then, for each pair (i,j) of channels, we computed the modulus of the time averaged phase difference mapped onto the unit circle:

$$PLV_{ij} = \left| \frac{1}{T} \sum_t e^{i(\phi_i^a(t) - \phi_j^a(t))} \right|$$

As with wSMI, we computed the PLV at trial level for each pair of electrodes, and then, for topographical representation, we computed the median PLV per EEG channel per trial.

Event-related potentials (ERPs) elicited by visual stimuli during the task

In order to study the neural fate of visual stimuli (digits and faces) during the SART task as a function of mind state, we conducted an event-related potential analysis on "Target epochs" (-0.25 to 0.75 s relative to stimulus onset). We first applied a baseline correction relative to the -0.25 to 0s time interval. Given the unbalanced nature of our dataset (important variability of the distribution of mind states across participants), we performed a single-trial multi-level analysis of ERPs responses[86] (see Statistics section for more details about this analysis). Before statistical analysis, to reduce inter-subject variability and to better fit the statistical model, we normalized channel voltages independently for each subject, by subtracting to each point of the *channel x time* matrix the mean *m* and dividing the result by the standard deviation *s*, with *m* and *s* being computed across all points of the *channel x time* matrix. Given that trials follow one another in close succession, it is normal for the baseline activity to be influenced by the activity of the previous trials as seen in Figure 4.

As a control, we also conducted the previously described analysis for each stimulus type (Faces vs. Digits) separately (see Figure S3).

Temporal decoding of stimulus type

To further study the neural fate of the visual stimuli as a function of mind state, we assessed whether we could decode stimulus type (Faces vs. Digits) from brain responses using multivariate pattern analysis (MVPA), with temporal decoding methods[43,68,87]. Briefly, this type of analysis consists in using a subset of the data to train a linear classifier at each time-point to differentiate trials where a *Face* was presented from trials where a *Digit* was presented, and then testing its performance, independently at each time-point, in a different subset of the data.

This method provides statistics tracking the temporal dynamics of mental representations. In the present study, we were interested in the differential profile of the temporal dynamics of mental representations related to external stimuli, as a function of the subject's mind-states (ON,MW and MB).

First, to avoid potential biases related to an unbalanced number of trials between mind-states (example: significantly more trials belonging to the ON mind state would induce better classifier performance in this condition than in the MB condition, independently of differential neural stimulus processing between conditions), we randomly downsampled, for each subject, the number of trials, so each mind state was equally represented. Then, independently for each reported mind-state (ON, MW, MB), we standardized the data at the subject level to suppress interindividual variability. At each time sample, and independently for each channel, channel voltages were standardized across trials sampled from the same participant, by removing the mean and scaling to unit variance. We then trained a linear classifier to decode Digits vs. Faces, using an L2-regularized (C=1) logistic regression, in a 10-fold cross-validation procedure. In each fold, all the trials were shuffled in a pseudo-randomized manner and split into a training set (9/10 of the trials) and a testing set (1/10 of the trials). The classifier's features were the standardized channel amplitudes. This training procedure was applied at each time step independently. Following the temporal decoding approach, the model trained at each time step was then tested at the same time-step on the testing set trials, at each cross-validation fold. The classifier performance at each testing time was evaluated by the area under the receiver operating curve (AUC) at each cross-validation fold. Global performance for each condition and at each time point was obtained by averaging the AUCs across folds. At each time point, performance against chance level was computed (see Statistics section). For visualization purposes, performance curves in function of time were smoothed using a gaussian filter, this filter wasn't applied for statistical analysis.

Decoding of mind-state using dimensionality reduction and a Random Forest classifier

Training and testing the classifier on labeled trials

We set out to determine if the participant's mind state could be predicted based on brain activity, on a trial-by-trial basis, using machine learning classifiers. We first focused on "Labeled Target" epochs, where the participant's mind state was considered as known (trials in the 5 seconds before subjective reports). From these epochs, we extracted the previously described EEG metrics (spectral, complexity, and connectivity, see "Calculation of electroencephalographic markers tracking cognitive modifications" section). We also added

two supplementary features, the mean channel voltages during the early time-period (100 ms to 300ms relative to trial onset) and the mean channel voltages during the late time-period (400-600ms relative to trial onset). For all the previously mentioned markers, we extracted for each trial the values of these markers for each EEG channel (obtaining thus 14 x 64 = 896 features). Given the very high dimensionality of our feature space, we implemented a dimensionality reduction technique prior to classification, using a non-linear (kernel) Principal Component Analysis (PCA)[88]. Classification was performed afterwards using Random Forest Classifiers. To take into account individual variability in neural metrics, we trained and tested a PCA/Random Forest classifier independently per participant, the hyperparameters of the PCA (Kernel type, number of components) and of the Random Forest (number of estimators, criterion, maximum depth) being fitted independently for each participant (see below). Importantly, to ensure an appropriate number of components/number of features ratio, the number of PCA components was chosen in the interval [2,25], corresponding therefore to a ratio of 1 component/10 trials or less, and hence avoiding overfitting. Kernel type was chosen from a list including the following Kernels: Linear, Polynomial, RBF and Sigmoid.

To find the best hyperparameters for our PCA/Random Forest pipeline, while also avoiding overfitting, we adopted a “Randomized Grid Search/Cross-validation procedure”, using 100 iterations. We performed this procedure for each participant. In each iteration, a combination of parameter settings was randomly sampled from all specified possible values of each parameter, then the PCA/Random Forest classifier was trained and tested by cross-validation (see below). At the end of all iterations, the set of hyperparameters that obtained the best cross-validated score (balanced accuracy, see below) was selected for further analyses. Comparison to chance level performance was obtained using a 500-permutation procedure, independently for each participant. First, the true classifier’s score was obtained by training and testing the best model (best set of hyperparameters) by cross validation. Then, at each permutation, trial labels were randomly shuffled, and the entire cross-validation procedure was repeated. We thus obtained a distribution of chance-level scores, for each participant. For each participant, we estimated the individual significance against chance by computing a p-value (by counting the number of permutation scores equal or higher to the true score and dividing it by the number of permutations plus one). Group-level significance against chance was also computed, by comparing the distribution of the classifiers' true scores across participants to the distribution of the mean permutation scores across participants (see Statistics section).

Cross-validation was performed using a 5-stratified group fold strategy. In each fold, 4/5 segments of the data were used to train the classifier and the remaining segment was used to

test the classifier (computation of the balanced accuracy score, see below). Note that class distributions (proportion of ON, MW, and MB trials) were preserved across partitions of the data. Note also that folds were grouped by experimental block (6 block per participant): the blocks that served for the training were not used for the testing. This was done to avoid overfitting linked to temporal proximity of epochs (trials) situated in the same experimental blocks. Note also that this group parameter (experimental block) was also used during the permutation procedure (labels were shuffled inside each block), to avoid over-estimation of significance against chance. At the end of the cross-validation procedure, mean performance scores were obtained by averaging the values obtained in each fold.

We computed a performance score adapted to unbalanced datasets such as ours (unbalanced number of ON, MW, and MB trials): the balanced accuracy score. The balanced accuracy is defined, in multi-class classification, as the average sensitivity Se ("How many relevant items are retrieved?") for each class. The sensitivity is computed as the number of true positives, divided by the number of true positives plus false negatives. Hence, the balanced accuracy (BA) was computed in our dataset according to the following formula:

$$_{BA} = \frac{Se_{ON} + Se_{MW} + Se_{MB}}{3}$$

$$= \frac{(TP/TP+FN)_{ON} + (TP/TP+FN)_{MW} + (TP/TP+FN)_{MB}}{3}$$

Note again that all the previously presented steps were performed using the Labeled Target epochs, where the participant's mind state was considered as known (trials in the 5 second period before subjective reports).

We also computed other very used classification metrics, at subject level and for each class: the Se (also called recall), the precision (TP/TP+FP) and the F1-score ((precision x recall)/(precision + recall)).

Predicting behavioral performances in non-labeled trials

To further test the performances of our classifier, trained on labeled trials, we predicted the mind state in non-labeled trials (more than 5 seconds before probe onsets). Practicaly speaking, we first fitted individual models with labeled data, and then predicted the mind state in non-labeled trials. Given the very high number of non-labeled trials (n=182,970) and its associated computational cost, we randomly subsampled, independently for each subject, 10% of non-labeled trials, resulting in a total of 18,293 trials included in this analysis. To assess the accuracy of this prediction, we once again computed behavioral performances, but this time only on non-labeled trials, and compared the behavioral profile as a function of the mind-

state in non-labeled trials (according to the classifier's prediction), to the behavioral profile in labeled trials.

Source space analyses

Forward Model and Source Modeling

We used a constrained distributed model consisting of 15,000 current dipoles, constrained to the cortical mantle of a generic brain model obtained from the BrainStorm software package. EEG forward modeling was computed using a symmetric Boundary Element Method (BEM) head model. Current density maps were computed using a minimum norm imaging method[89].

Computation of wSMI and PLV at source level

We estimated the cortical sources of our "Probe epochs". We then extracted trial-to-trial source activity time series of a set of 68 cortical regions, according to a standard anatomical atlas (Desikan-Killiany[90]). Using the same method described for sensor space analysis, we computed the wSMI and the PLV between each pair of cortical regions (n=2278). Finally, to reduce the number of multiple comparisons and ease the interpretation of this analysis, we computed the median wSMI between pairs of regions of interest (ROIs). To do so, we grouped the 68 cortical regions in 5 pairs of ROIs, according to the Desikan-Killiany atlas (frontal, limbic, temporal, parietal and occipital). The wSMI/PLV between two ROIs was computed as the median across all the connections shared by the two ROIs. We hence computed a wSMI or PLV value for each pair of ROIs (n=45 connections) and each trial, at each frequency band for the wSMI (delta, theta, alpha, beta and gamma).

Source estimation of stimulus evoked activity

We also estimated the cortical sources of our "Target epochs". Independently for each condition (mind state), we compared the stimulus evoked activity to baseline activity (at source level) using a t-test against the baseline period (see Statistics section).

Statistics

Analyses are listed by order of apparition in the results section

Behavior

We compared the rate of Misses and FA between mind states at trial level using binomial generalized linear mixed models, with mind state as the explanatory factor and with two random factors (random intercepts): **subject ID and dataset (Monash dataset and Paris Brain Institute dataset**). For each behavioral measure and each mind state, response probability and confidence intervals (95%) were back-transformed from the logit scale. For RTs, we used a (gaussian) linear mixed model with mind state as the explanatory factor and s**ubject ID and dataset as random intercepts.** Subject ID is nested within dataset as each subject belongs to only one dataset. Estimated marginal means and confidence intervals (95%) of RTs for each mind state were extracted from the model. All p-values were corrected for multiple comparisons using a *False Discovery Rate* (FDR) procedure, with an alpha level at 0.05 (5%) (for n= 24 comparisons) .

Sensor space EEG markers

For each previously described EEG marker, we compared the three mind states (ON, MW, MB) using linear mixed models at trial level, with mind state, EEG sensor (n=64) and their interaction as explanatory factors, and two random factors (random intercepts), subject identity and dataset (Monash dataset and Paris Brain Institute dataset). Marker values were standardized (z-scored) across all trials before statistical analysis to better fit the linear mixed models. ANOVA tables were computed from the models. We computed post-hoc contrasts between mind states (model estimates and statistical comparisons) at each EEG sensor. During this post-hoc analysis, to reduce the effect of possibly spurious outliers, we applied a winsorizing procedure to all contrast estimates and uncorrected p-values, were the contrast minima and maxima, as well as the p-value minima were limited to values between -5 and +5 T-values. All p-values were corrected for multiple comparisons using an FDR procedure. Main factor's p-values were corrected across the number of factors and the total number of EEG statistical models (n_factors x n_models= 3x (10 state markers + 4 source space connectivity measured + 10 ERPs time windows = 3 x 24 = 72 comparisons, alpha level = 0.05). Post-hoc p-values for each EEG marker were corrected after winsorization across the number of EEG sensors and the number of conditions (correction for n_sensors x n_conditions= 64 x 3=192 comparisons, alpha level = 0.05) .

As a control analysis, we also computed statistical models including the vigilance score, and its interaction with electrode location, as covariates, all other factors and parameters being kept identical as previously described.

Source space wSMI

For each frequency band, we performed a linear mixed model at trial level, with mind state, connection id (ROI1-ROI2) (n=45) and their interaction as explanatory factors, and the same random intercepts (subject identity and dataset). As before, we computed ANOVA tables and post-hoc contrasts between mind-states for each pair of source ROIs, correcting all p-values for multiple comparisons using an FDR procedure, as described above (correction for 72 comparisons for models' main factors, and for n_conditions x n_connections = 3 x 45 = 135 comparisons for each connectivity metric post-hoc p-values)

As a control analysis, we also computed statistical models including the vigilance score, and its interaction with connection identity, as covariates, all other factors and parameters being kept identical as previously described

Sensor space ERPs

We performed a mass-univariate (across time and space dimensions) single-trial multi-level analysis of ERPs responses. We initially intended to add both *EEG channel* and *time* (in addition to *mind state*) as factors to the same mixed linear model, but this was not feasible for computational reasons. We therefore subsampled our time dimension (-250 to 750 ms relative to stimuli onsets) by using a -25 to +25ms sliding time-window, with 75ms steps, resulting in a set of 10 time-windows of interest. We then performed a linear mixed model for each time-window, with *channel amplitude* as the dependent factor; *mind state*, *EEG sensor* and their interaction as explanatory factors; and subject ID and dataset as a random factors (random intercepts). Models' main factors' p-values were corrected for the total number of EEG statistical models x number of factors = 72 comparisons (FDR procedure, alpha level= 0.05). For each time-window, voltage estimates for each mind state, and their statistical comparisons, were computed for each EEG sensor. All obtained p-values were corrected for multiple comparisons using an FDR procedure (for n_sensors x n_conditions x n_times = 64 x 3 x 10 = 1920 comparisons, alpha level = 0.05).

Temporal decoding

For each mind-state, classification performance at each time point was tested against chance level performance using a two-sided non-parametric test (Mann-Whitney) across validation folds (distribution of scores across folds compared to a dummy beta distribution centered around 0.5, with alpha = beta= 20). These statistics were then corrected for multiple comparisons using an FDR procedure (for n_times X n_conditions= 251 x 3= 753 comparisons, alpha level = 0.05).

Source estimation of stimulus evoked activity

We performed a t-test against baseline at each time sample and each cortical source, and corrected for multiple comparisons across time, space and frequency dimensions using an FDR procedure (alpha=0.0001).

Comparison to chance level performance of the classifier trained to distinguish different mind states

As already explained in the previous sections, we compared our classifiers' performances to chance level using a 500-permutation procedure. We performed this procedure for each participant. At each permutation, trial labels were randomly shuffled (grouped by experimental blocks), then the entire training/testing cross-validation procedure was repeated, using the hyperparameters previously selected during the grid search procedure. We thus obtained a distribution of chance-level scores, for each participant. To calculate the individual p-value, we counted the number of permutation scores equal or higher to our true score and divided it by the number of permutations plus one. To assess group level statistical significance against chance, we performed a two-tailed Wilcoxon rank sum test, where we compared the distribution of true classification scores across participants (non permuted data), to the distribution of mean permutation scores (permuted data) across participants.

Software

Most analyses were performed in Python 3.9.13 , using the following packages:

- MNE (v 1.4.2) (https://mne.tools/stable/index.html): preprocessing and manipulation of EEG data
- MNE-features (v 0.2.1) (https://mne.tools/mne-features/) and nice-tools (https://github.com/nice-tools/nice): computation of EEG neural markers
- Pymer4 (v 0.8.0) (https://eshinjolly.com/pymer4/) and pingouin (v 0.5.3) (https://pingouin-stats.org/build/html/index.html) : statistical analysis
- Scikit-learn (v 1.3) (https://scikit-learn.org/stable/) : machine learning analyses

Binomial mixed models (for behavioral analyses) were performed in R using the *lme4* and *emmeans* libraries.

Source reconstruction analyses were performed in Matlab using the Brainstorm package (https://neuroimage.usc.edu/brainstorm/Introduction)

For the Monash dataset, initial preprocessing of raw EEG files using ICA was performed in Matlab using EEGlab 2021.1 and FieldTrip-20210807.

REFERENCES

1. James, W. *The Principles of Psychology*. (Henry Holt and Company, New York, 1890).

2. Smallwood, J., Obonsawin, M. & Heim, D. Task unrelated thought: the role of distributed processing. *Conscious Cogn* **12**, 169–189 (2003).

3. Smallwood, J. & Schooler, J. W. The Science of Mind Wandering: Empirically Navigating the Stream of Consciousness. *Annual Review of Psychology* **66**, 487–518 (2015).

4. Gruberger, M., Simon, E., Levkovitz, Y., Zangen, A. & Hendler, T. Towards a Neuroscience of Mind-Wandering. *Frontiers in Human Neuroscience* **5**, (2011).

5. Compton, R. J., Gearinger, D. & Wild, H. The wandering mind oscillates: EEG alpha power is enhanced during moments of mind-wandering. *Cogn Affect Behav Neurosci* **19**, 1184–1191 (2019).

6. Braboszcz, C. & Delorme, A. Lost in thoughts: neural markers of low alertness during mind wandering. *Neuroimage* **54**, 3040–3047 (2011).

7. Andrillon, T., Burns, A., Mackay, T., Windt, J. & Tsuchiya, N. Predicting lapses of attention with sleep-like slow waves. *Nat Commun* **12**, 3657 (2021).

8. Schooler, J. W. *et al.* Meta-awareness, perceptual decoupling and the wandering mind. *Trends in Cognitive Sciences* **15**, 319–326 (2011).

9. Ward, A. & Wegner, D. Mind-blanking: when the mind goes away. *Frontiers in Psychology* **4**, (2013).

10. Schooler, J. W., Reichle, E. D. & Halpern, D. V. Zoning Out while Reading: Evidence for Dissociations between Experience and Metaconsciousness. in *Thinking and seeing: Visual metacognition in adults and children* 203–226 (MIT Press, Cambridge, MA, US, 2004).

11. Van Calster, L., D'Argembeau, A., Salmon, E., Peters, F. & Majerus, S. Fluctuations of Attentional Networks and Default Mode Network during the Resting State Reflect Variations in Cognitive States: Evidence from a Novel Resting-state Experience Sampling Method. *Journal of Cognitive Neuroscience* **29**, 95–113 (2017).

12. Kaufmann, A., Parmigiani, S., Kawagoe, T., Zabaroff, E. & Wells, B. Two models of mind blanking. *Eur J of Neuroscience* ejn.16164 (2023) doi:10.1111/ejn.16164.

13. Fell, J. What is mind blanking: A conceptual clarification. *Eur J of Neuroscience* **56**, 4837–4842 (2022).

14. Boulakis, P. A. & Demertzi, A. Relating mind-blanking to the content and dynamics of spontaneous thinking. *Current Opinion in Behavioral Sciences* **61**, 101481 (2025).

15. Boulakis, P. A., Mortaheb, S., Van Calster, L., Majerus, S. & Demertzi, A. Whole-Brain Deactivations Precede Uninduced Mind-Blanking Reports. *J. Neurosci.* **43**, 6807–6815 (2023).

16. Kawagoe, T., Onoda, K. & Yamaguchi, S. The neural correlates of "mind blanking": When the mind goes away. *Human Brain Mapping* **40**, 4934–4940 (2019).

17. Mortaheb, S. *et al.* Mind blanking is a distinct mental state linked to a recurrent brain profile of globally positive connectivity during ongoing mentation. *Proceedings of the National Academy of Sciences* **119**, e2200511119 (2022).

18. Mittner, M., Hawkins, G. E., Boekel, W. & Forstmann, B. U. A Neural Model of Mind Wandering. *Trends in Cognitive Sciences* **20**, 570–578 (2016).

19. Unsworth, N. & Robison, M. K. Tracking arousal state and mind wandering with pupillometry. *Cogn Affect Behav Neurosci* **18**, 638–664 (2018).

20. Andrillon, T. *et al.* Does the Mind Wander When the Brain Takes a Break? Local Sleep in Wakefulness, Attentional Lapses and Mind-Wandering. *Frontiers in Neuroscience* **13**, (2019).

21. Andrillon, T., Lutz, A., Windt, J. & Demertzi, A. Where is my Mind?: A Neurocognitive Investigation of Mind Blanking. Preprint at https://doi.org/10.31234/osf.io/xmtga (2024).

22. Boulakis, P. A. & Demertzi, A. Relating mind-blanking to the content and dynamics of spontaneous thinking. *Current Opinion in Behavioral Sciences* **61**, 101481 (2025).

23. Siclari, F., LaRocque, J., Postle, B. & Tononi, G. Assessing sleep consciousness within subjects using a serial awakening paradigm. *Frontiers in Psychology* **4**, (2013).

24. Siclari, F. *et al.* The neural correlates of dreaming. *Nature Neuroscience* **20**, 872–878 (2017).

25. Türker, B. *et al.* Behavioral and brain responses to verbal stimuli reveal transient periods of cognitive integration of the external world during sleep. *Nat Neurosci* **26**, 1981–1993 (2023).

26. Mazza, S. *et al.* Asleep but aware? *Brain and Cognition* **87**, 7–15 (2014).

27. Andrillon, T. & Kouider, S. The vigilant sleeper: neural mechanisms of sensory (de)coupling during sleep. *Current Opinion in Physiology* **15**, 47–59 (2020).

28. Dehaene, S. Towards a cognitive neuroscience of consciousness: basic evidence and a workspace framework. *Cognition* **79**, 1–37 (2001).

29. Mashour, G. A., Roelfsema, P., Changeux, J.-P. & Dehaene, S. Conscious Processing and the Global Neuronal Workspace Hypothesis. *Neuron* **105**, 776–798 (2020).

30. Tononi, G. & Massimini, M. Why does consciousness fade in early sleep? *Ann N Y Acad Sci* **1129**, 330–334 (2008).

31. Casali, A. G. *et al.* A Theoretically Based Index of Consciousness Independent of Sensory Processing and Behavior. *Science Translational Medicine* **5**, 198ra105-198ra105 (2013).

32. Casarotto, S. *et al.* Exploring the Neurophysiological Correlates of Loss and Recovery of Consciousness: Perturbational Complexity. in *Brain Function and Responsiveness in Disorders of Consciousness* (eds. Monti, M. M. & Sannita, W. G.) 93–104 (Springer International Publishing, Cham, 2016). doi:10.1007/978-3-319-21425-2_8.

33. Sitt, J. D. *et al.* Large scale screening of neural signatures of consciousness in patients in a vegetative or minimally conscious state. *Brain* **137**, 2258–2270 (2014).

34. Engemann, D. A. *et al.* Robust EEG-based cross-site and cross-protocol classification of states of consciousness. *Brain* **141**, 3179–3192 (2018).

35. Boveroux, P. *et al.* Breakdown of within- and between-network resting state functional magnetic resonance imaging connectivity during propofol-induced loss of consciousness. *Anesthesiology* **113**, 1038–1053 (2010).

36. Ranft, A. *et al.* Neural Correlates of Sevoflurane-induced Unconsciousness Identified by Simultaneous Functional Magnetic Resonance Imaging and Electroencephalography. *Anesthesiology* **125**, 861–872 (2016).

37. Horovitz, S. G. *et al.* Decoupling of the brain's default mode network during deep sleep. *Proc Natl Acad Sci U S A* **106**, 11376–11381 (2009).

38. Spoormaker, V. I. *et al.* Development of a large-scale functional brain network during human non-rapid eye movement sleep. *J Neurosci* **30**, 11379–11387 (2010).

39. King, J.-R. *et al.* Information Sharing in the Brain Indexes Consciousness in Noncommunicative Patients. *Current Biology* **23**, 1914–1919 (2013).

40. Bourdillon, P. *et al.* Brain-scale cortico-cortical functional connectivity in the delta-theta band is a robust signature of conscious states: an intracranial and scalp EEG study. *Scientific Reports* **10**, 1–13 (2020).

41. Bekinschtein, T. A. *et al.* Neural signature of the conscious processing of auditory regularities. *PNAS* **106**, 1672–1677 (2009).

42. Perez, P. *et al.* Auditory Event-Related "Global Effect" Predicts Recovery of Overt Consciousness. *Frontiers in Neurology* **11**, (2021).

43. King, J.-R., Gramfort, A., Schurger, A., Naccache, L. & Dehaene, S. Two Distinct Dynamic Modes Subtend the Detection of Unexpected Sounds. *PLoS ONE* **9**, e85791 (2014).

44. Strauss, M. *et al.* Disruption of hierarchical predictive coding during sleep. *Proceedings of the National Academy of Sciences* **112**, E1353–E1362 (2015).

45. Hayat, H. *et al.* Reduced neural feedback signaling despite robust neuron and gamma auditory responses during human sleep. *Nat Neurosci* **25**, 935–943 (2022).

46. Pérez, P. *et al.* Content–state dimensions characterize different types of neuronal markers of consciousness. *Neuroscience of Consciousness* **2024**, niae027 (2024).

47. Van den Driessche, C. *et al.* Attentional Lapses in Attention-Deficit/Hyperactivity Disorder: Blank Rather Than Wandering Thoughts. *Psychol Sci* **28**, 1375–1386 (2017).

48. Richman, J. S. & Moorman, J. R. Physiological time-series analysis using approximate entropy and sample entropy. *American Journal of Physiology-Heart and Circulatory Physiology* **278**, H2039–H2049 (2000).

49. Engemann, D. A. *et al.* Robust EEG-based cross-site and cross-protocol classification of states of consciousness. *Brain* **141**, 3179–3192 (2018).

50. Schartner, M. M. *et al.* Global and local complexity of intracranial EEG decreases during NREM sleep. *Neuroscience of Consciousness* **2017**, (2017).

51. Türker, B. *et al.* Behavioral and brain responses to verbal stimuli reveal transient periods of cognitive integration of external world in all sleep stages. 2022.05.04.490484 Preprint at https://doi.org/10.1101/2022.05.04.490484 (2022).

52. Munoz Musat, E., Rohaut, B., Sangare, A., Benhaiem, J.-M. & Naccache, L. Hypnotic Induction of Deafness to Elementary Sounds: An Electroencephalography Case-Study and a Proposed Cognitive and Neural Scenario. *Frontiers in Neuroscience* **16**, (2022).

53. Martínez Vivot, R., Pallavicini, C., Zamberlan, F., Vigo, D. & Tagliazucchi, E. Meditation Increases the Entropy of Brain Oscillatory Activity. *Neuroscience* **431**, 40–51 (2020).

54. Boulakis, P. A. *et al.* Variations of autonomic arousal mediate the reportability of mind blanking occurrences. *Sci Rep* **15**, 4956 (2025).

55. Bastuji, H. & García-Larrea, L. Evoked potentials as a tool for the investigation of human sleep. *Sleep Med Rev* **3**, 23–45 (1999).

56. Ruby, P., Caclin, A., Boulet, S., Delpuech, C. & Morlet, D. Odd sound processing in the sleeping brain. *J Cogn Neurosci* **20**, 296–311 (2008).

57. Nir, Y., Vyazovskiy, V. V., Cirelli, C., Banks, M. I. & Tononi, G. Auditory responses and stimulus-specific adaptation in rat auditory cortex are preserved across NREM and REM sleep. *Cereb Cortex* **25**, 1362–1378 (2015).

58. Kouider, S., Andrillon, T., Barbosa, L. S., Goupil, L. & Bekinschtein, T. A. Inducing Task-Relevant Responses to Speech in the Sleeping Brain. *Current Biology* **24**, 2208–2214 (2014).

59. Andrillon, T., Poulsen, A. T., Hansen, L. K., Léger, D. & Kouider, S. Neural Markers of Responsiveness to the Environment in Human Sleep. *J. Neurosci.* **36**, 6583–6596 (2016).

60. Fischer, C. *et al.* Mismatch negativity and late auditory evoked potentials in comatose patients. *Clinical Neurophysiology* **110**, 1601–1610 (1999).

61. Fischer, C., Luauté, J., Adeleine, P. & Morlet, D. Predictive value of sensory and cognitive evoked potentials for awakening from coma. *Neurology* **63**, 669–673 (2004).

62. Robinson, L. R., Micklesen, P. J., Tirschwell, D. L. & Lew, H. L. Predictive value of somatosensory evoked potentials for awakening from coma*. *Critical Care Medicine* **31**, 960 (2003).

63. Sergent, C. *et al.* Bifurcation in brain dynamics reveals a signature of conscious processing independent of report. *Nat Commun* **12**, 1149 (2021).

64. Sergent, C., Baillet, S. & Dehaene, S. Timing of the brain events underlying access to consciousness during the attentional blink. *Nature Neuroscience* **8**, 1391–1400 (2005).

65. Del Cul, A., Baillet, S. & Dehaene, S. Brain Dynamics Underlying the Nonlinear Threshold for Access to Consciousness. *PLoS Biol* **5**, (2007).

66. Gaillard, R. *et al.* Converging Intracranial Markers of Conscious Access. *PLoS Biol* **7**, (2009).

67. Spehlmann, R. The averaged electrical responses to diffuse and to patterned light in the human. *Electroencephalogr Clin Neurophysiol* **19**, 560–569 (1965).

68. King, J.-R. *et al.* Encoding and Decoding Neuronal Dynamics: Methodological Framework to Uncover the Algorithms of Cognition. (2018).

69. Ward, A. F. & Wegner, D. M. Mind-blanking: when the mind goes away. *Front Psychol* **4**, 650 (2013).

70. Nisbett, R. E. & Wilson, T. D. Telling more than we can know: Verbal reports on mental processes. *Psychological Review* **84**, 231–259 (1977).

71. Rocchi, F. *et al.* Increased fMRI connectivity upon chemogenetic inhibition of the mouse prefrontal cortex. *Nat Commun* **13**, 1056 (2022).

72. Christoff, K., Gordon, A. M., Smallwood, J., Smith, R. & Schooler, J. W. Experience sampling during fMRI reveals default network and executive system contributions to mind wandering. *Proceedings of the National Academy of Sciences of the United States of America* **106**, 8719–8724 (2009).

73. Aydore, S., Pantazis, D. & Leahy, R. M. A note on the phase locking value and its properties. *NeuroImage* **74**, 231–244 (2013).

74. Imperatori, L. S. *et al.* EEG functional connectivity metrics wPLI and wSMI account for distinct types of brain functional interactions. *Sci Rep* **9**, 8894 (2019).

75. Aedo-Jury, F., Schwalm, M., Hamzehpour, L. & Stroh, A. Brain states govern the spatio-temporal dynamics of resting-state functional connectivity. *eLife* **9**, e53186 (2020).

76. El-Baba, M. *et al.* Functional connectivity dynamics slow with descent from wakefulness to sleep. *PLOS ONE* **14**, e0224669 (2019).

77. Aru, J., Bachmann, T., Singer, W. & Melloni, L. Distilling the neural correlates of consciousness. *Neuroscience & Biobehavioral Reviews* **36**, 737–746 (2012).

78. Tsuchiya, N., Wilke, M., Frässle, S. & Lamme, V. A. F. No-Report Paradigms: Extracting the True Neural Correlates of Consciousness. *Trends in Cognitive Sciences* **19**, 757–770 (2015).

79. Cohen, M. A., Ortego, K., Kyroudis, A. & Pitts, M. Distinguishing the Neural Correlates of Perceptual Awareness and Postperceptual Processing. *J. Neurosci.* **40**, 4925–4935 (2020).

80. Pitts, M. A., Metzler, S. & Hillyard, S. A. Isolating neural correlates of conscious perception from neural correlates of reporting one's perception. *Front Psychol* **5**, 1078 (2014).

81. Polich, J. Updating P300: An integrative theory of P3a and P3b. *Clinical Neurophysiology* **118**, 2128–2148 (2007).

82. Naccache, L. Why and how access consciousness can account for phenomenal consciousness. *Philosophical Transactions of the Royal Society B: Biological Sciences* **373**, 20170357 (2018).

83. Tononi, G. The Integrated Information Theory of Consciousness: An Updated Account. *Archives Italiennes de Biologie* **150**, 56–90 (2012).

84. Langner, O. *et al.* Presentation and validation of the Radboud Faces Database. *Cognition & Emotion* **24**, 1377–1388 (2010).

85. Kayser, J. & Tenke, C. E. Principal components analysis of Laplacian waveforms as a generic method for identifying ERP generator patterns: II. Adequacy of low-density estimates. *Clinical Neurophysiology* **117**, 369–380 (2006).

86. Volpert-Esmond, H. I., Merkle, E. C., Levsen, M. P., Ito, T. A. & Bartholow, B. D. Using Trial-Level Data and Multilevel Modeling to Investigate Within-Task Change in Event-Related Potentials. *Psychophysiology* **55**, e13044 (2018).

87. King, J.-R. & Dehaene, S. Characterizing the dynamics of mental representations: the temporal generalization method. *Trends in Cognitive Sciences* **18**, 203–210 (2014).

88. Weston, J., Schölkopf, B. & Bakir, G. Learning to Find Pre-Images. in *Advances in Neural Information Processing Systems* vol. 16 (MIT Press, 2003).

89. Baillet, S., Mosher, J. C. & Leahy, R. M. Electromagnetic brain mapping. *IEEE Signal Processing Magazine* **18**, 14–30 (2001).

90. Desikan, R. S. *et al.* An automated labeling system for subdividing the human cerebral cortex on MRI scans into gyral based regions of interest. *NeuroImage* **31**, 968–980 (2006).

Acknowledgments:

AWC acknowledges the support of the Three Springs Foundation. The research leading to these results has received funding from the national program “Investissements d’avenir” ANR-10- IAIHU-0006. Part of this work was carried out in the CENIR of ICM. We gratefully acknowledge Laurent Hugueville and Amandine Carrie for their contribution to data collection at the Paris Brain Institute. We thank Teigane Mackay for data collection at Monash University, Naotsugu Tsuchiya, and Jennifer Windt for their support to TA at the inception of this line of research, and Jakob Howhy, Delphine Oudiette and Jacobo Sitt for the discussion about the nature and dynamics of consciousness.

Funding:

European Research Council ERC-StG SleepingAwake 101116748 (TA)

Agence Nationale de la Recherche ANR-22-CE37–0006-01 (TA)

Human Frontiers Science Program LT000362/2018-L (TA)

Author contributions:

Conceptualization: EMM, AWC, LN, TA

Data acquisition: ALC, TA

Methodology: EMM, AWC, LB, LN, TA

Investigation: EMM, TA

Visualization: EMM, TA

Funding acquisition: LN, TA

Supervision: LN, TA

Writing – original draft: EMM

Writing – review & editing: EMM, ALC, AWC, LB, LN, TA

Competing interests:

Authors declare that they have no competing interests.

Data and materials availability:

All data, code, and materials used in the analysis will be freely available upon publication.

FIGURES

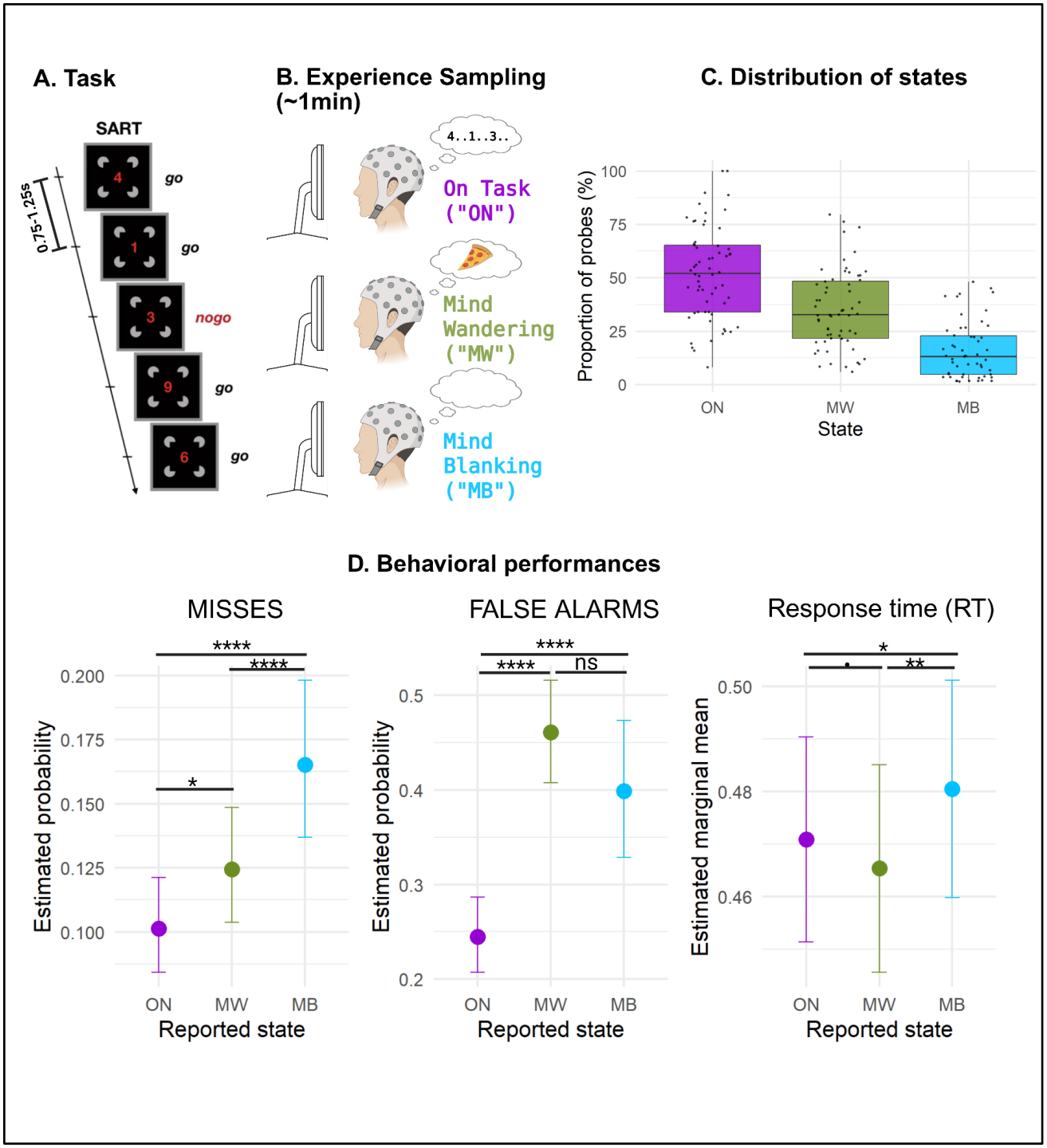

Figure 1: Experimental paradigm and behavioral results. Panels A and B: Experimental paradigm. 62 healthy participants performed a sustained attention to response task (SART), with digits and faces as stimuli, while high-density electro-encephalogram (EEG) was recorded continuously. After each stimulus presentation, participants had to press a button (Go trials), or refrain from doing so, whenever a "3" or a smiling face was presented (No Go trials; 1 out of 9). SOA varied randomly (750-1250ms) with a null ISI (panel A). Participants' mental state was probed at random intervals (every 40-70s, uniform random jitter). They had to report their attentional focus by selecting one of four options: (1) 'task-focused' (ON), (2) 'off-task' (mind-wandering, MW), (3) 'mind-blanking' (MB) (panel B). Panel C: proportion of probes in function of the reported mind-state. Proportions were computed at subject level (individual dots) and the distributions at group level are represented by a boxplot (the boundaries of the boxes represent first and third quartiles (Q1 and Q3 respectively), mid-line represents the medium and the whiskers depict Q1-1.5*IQR and Q3*1.5*IQR). Panel D: Behavioral performances in function of the reported mind-state. Misses, False Alarms and Response Times (RT) were computed for the trials between the 5s before probe-onsets. (Binomial) linear mixed models were computed with *mind-state* as the main explanatory factor, and subject ID/dataset as a random intercepts. We found fine-grained modulations of performance in function of mind-state, with distinct behavioral profiles for MW (faster RTs) and MB (slower RTs, more misses). The statistical bars and stars represent the pairwise comparisons between mind-states (FDR corrected). The detailed statistical results can be found on Table 1.

****: FDR corrected p-value<0.0001

**: FDR corrected p-value<0.01

*: FDR corrected p-value<0.05

. : FDR corrected p-value<0.1

n.s. FDR corrected p-value>0.1

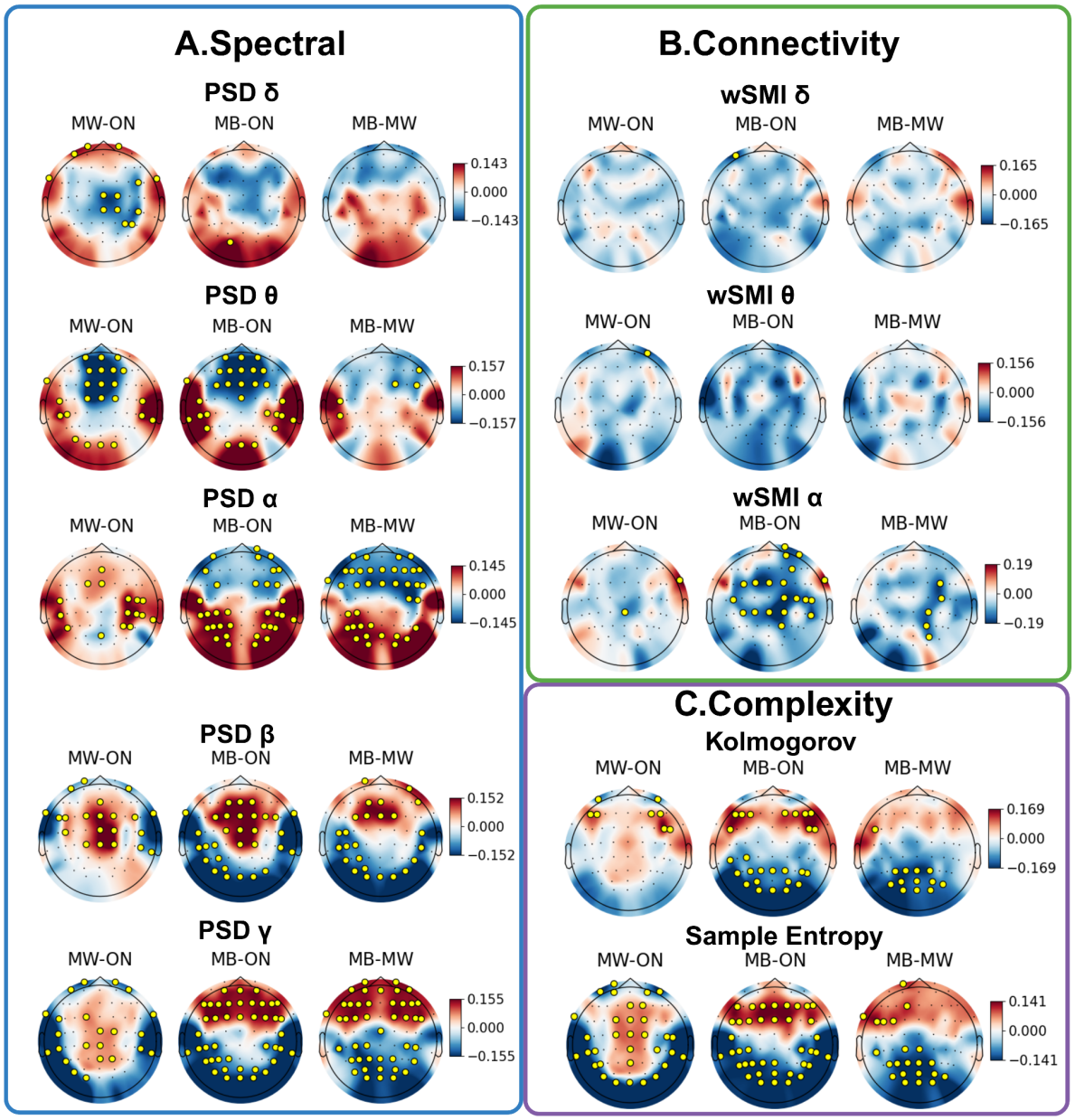

Figure 2: EEG-based neurophysiological markers differentiate MB from ON and MW. Spectral (A), Connectivity (B) and Complexity (C) results. Each subplot represents the pairwise statistical contrast between two states (left: MW - ON; middle: MB - ON; right: MB - MW), at sensor level (topographical representation of the scalp). Model estimates for the contrast between states were computed for each electrode, and locations with statistically significant differences (FDR corrected p-value<0.05) are depicted with a golden circle. We observed a front-back dissociation between MW and MB for spectral and complexity measures, and a progressive breakdown of functional connectivity going from ON to MB (ON>MW>MB). The ANOVA tables summarizing the main factor's effects (linear mixed models with mind-state, electrode/connection and their interaction as main factors, and subject ID/dataset as a random intercepts) for each EEG metric can be found in Table 2.

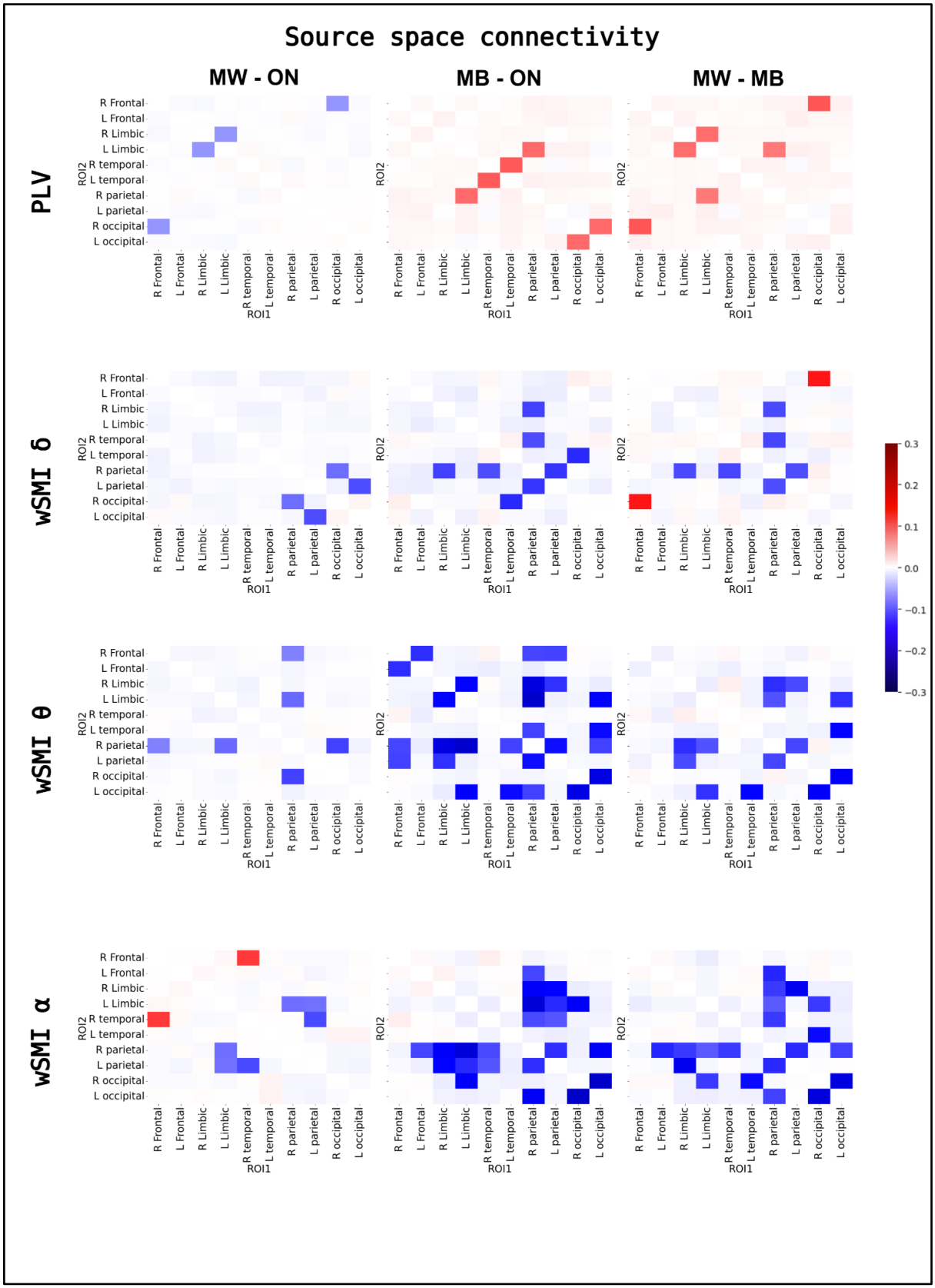
Source space connectivity
MW - ON
MB - ON
MW - MB
PLV
wSMI δ
wSMI θ
wSMI α
ROI1
ROI2
R Frontal
L Frontal
R Limbic
L Limbic
R temporal
L temporal
R parietal
L parietal
R occipital
L occipital
0.3
0.2
0.1
0.0
−0.1
−0.2
−0.3

Figure 3: Increased phase synchrony with reduced information sharing during MB. The PLV (top) and the wSMI in different frequency bands were computed at the source level. Each square-matrix represents the contrast in connectivity, computed in source space, between two mind-states, for each pair of regions of interest (ROIs). Only significantly different connections (FDR corrected p-value<0.05) are highlighted, the other ones are masked. ANOVA tables for the statistical models can be found in Table 3. We observed a dissociation between the PLV and wSMI, with increased PLV (phase synchrony) and decreased wSMI (information sharing) between distant cortical areas (in particular fronta-parietal) during MB, as compared to ON and MW.

δ: delta band; θ: theta band; α: alpha band
wSMI: weighted symbolic mutual information
PLV: Phase Locking Value
R: right; L: left

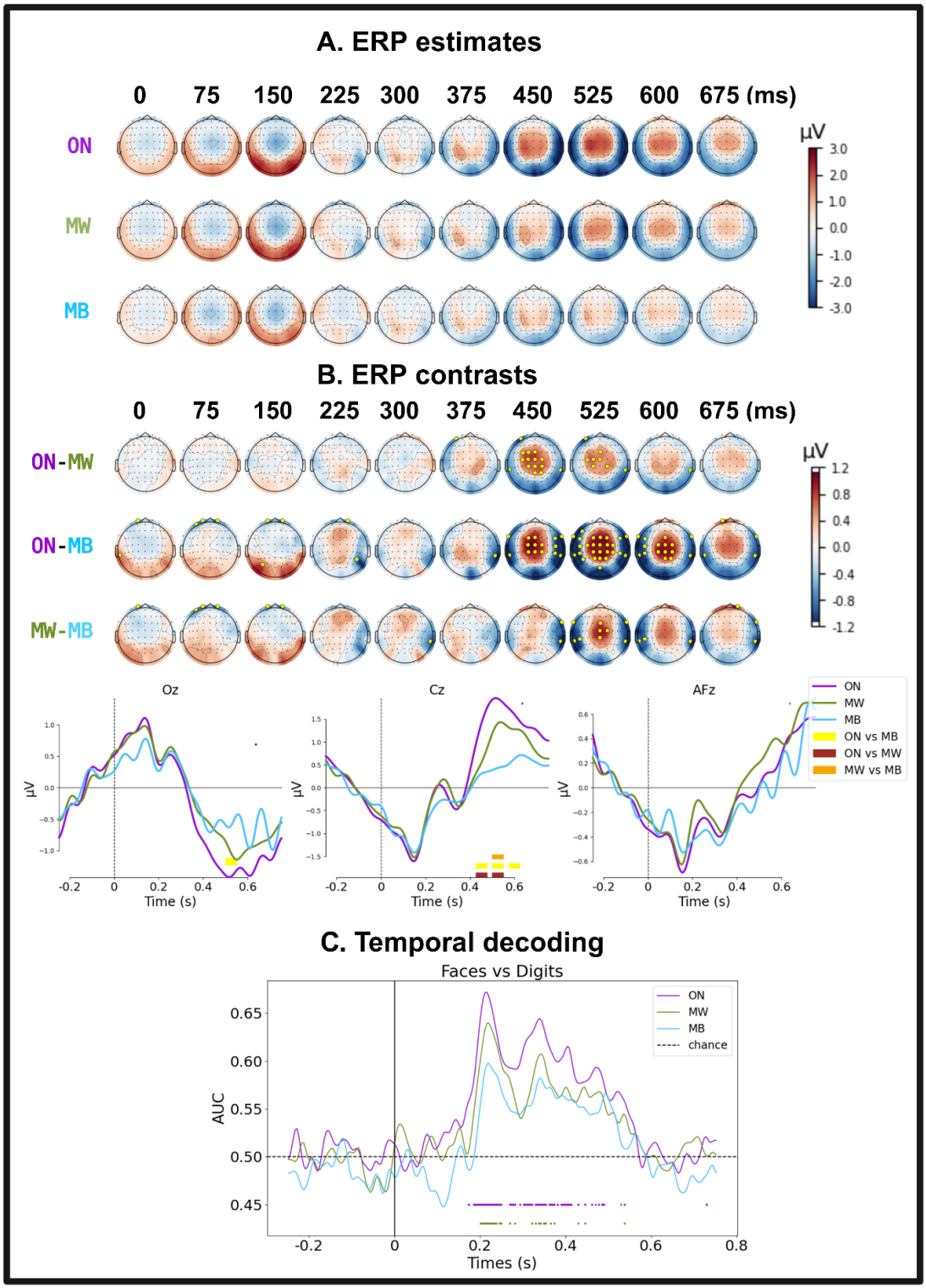
A. ERP estimates
0 75 150 225 300 375 450 525 600 675 (ms)
ON
MW
MB
µV
3.0
2.0
1.0
0.0
-1.0
-2.0
-3.0
B. ERP contrasts
0 75 150 225 300 375 450 525 600 675 (ms)
ON-MW
ON-MB
MW-MB
µV
1.2
0.8
0.4
0.0
-0.4
-0.8
-1.2
Oz
Cz
AFz
µV
Time (s)
ON
MW
MB
ON vs MB
ON vs MW
MW vs MB
C. Temporal decoding
Faces vs Digits
AUC
0.65
0.60
0.55
0.50
0.45
-0.2
0
0.2
0.4
0.6
0.8
Times (s)
ON
MW
MB
chance

Figure 4: Stimulus-induced activity analyses. Panels A and B: Topographical scalp representation of the ERP estimates for each mind state (A) and ERP contrasts between mind-states (B), derived from the statistical model (single-trial multi-level analysis with mind-state, EEG channel and their interaction as main factors, and subject ID/dataset as random intercepts). Marked electrodes in panel B (golden circles) are the ones presenting a statistically significant difference between conditions (FDR corrected p-value<0.05). Panel B bottom presents the grand-average ERP time-series for each mind-state (ON: violet; MW: green; MB: blue) for 3 electrodes of interest (Oz, Cz and AFz). Time-points with statistically significant differences between conditions (FDR corrected p-value<0.05) are highlighted (ON vs MW: brown; ON vs MB: yellow; MW vs MB: orange). Given that trials follow one another in close succession, it is normal for the baseline activity to be influenced by the activity of the previous trials. Panel C: Temporal decoding of stimulus category. A linear classifier was trained and then tested (via cross validation) at each time point to distinguish stimulus category (Faces vs Digits), allowing the tracking of the temporal dynamics of neural representations, independently for each mind-state. Note that the number of trials were identical between mind-states for this analysis. Classifiers' performances were compared to chance-level performance (see Methods), independently for each mind-state, and statistically significant time-points were represented by colored horizontal bars. While both early (<300ms) and late (>300ms) time-points with significant decoding were observed for ON and MW, no significant decoding was observed for MB trials.

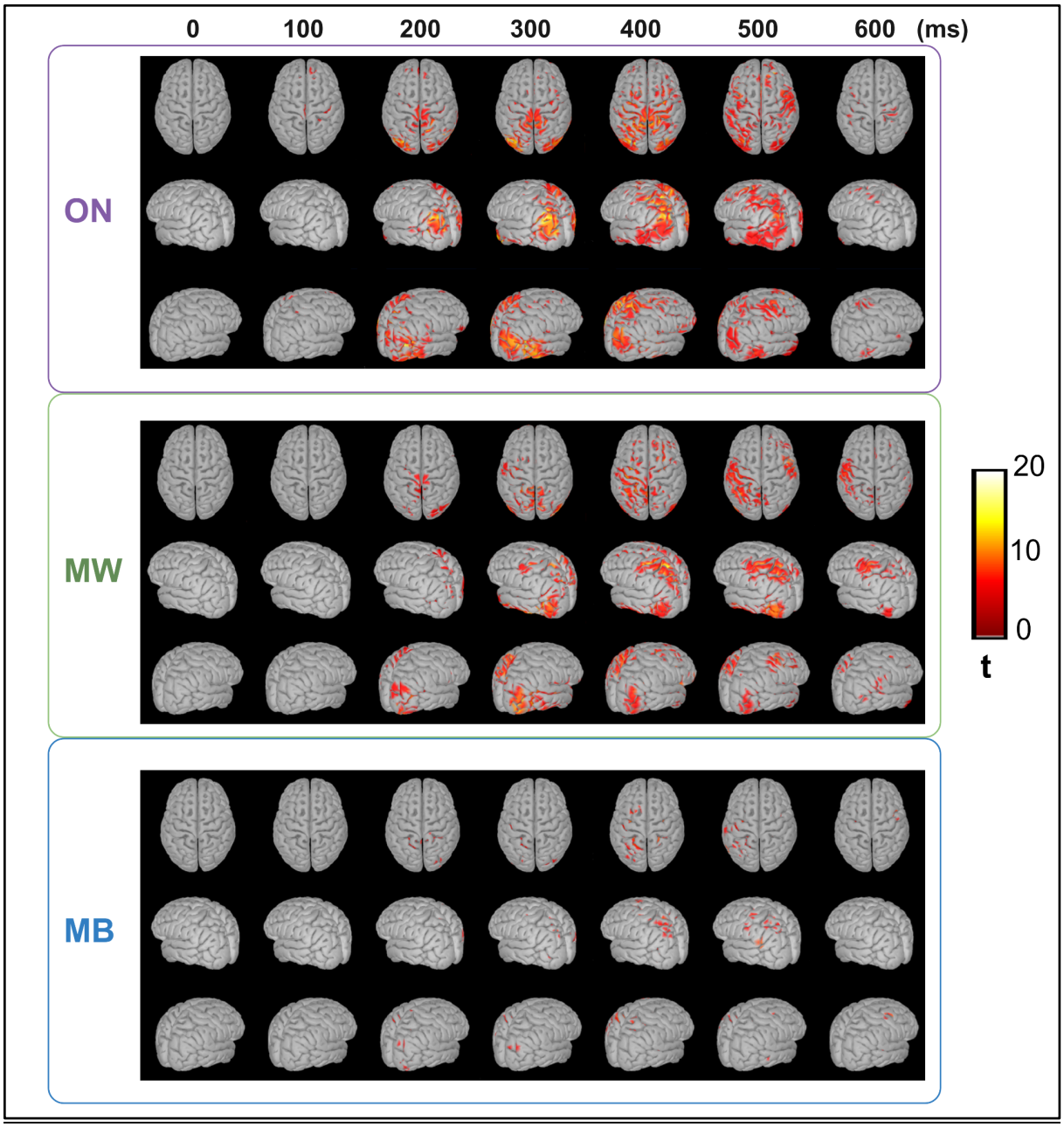

Figure 5: Source reconstruction of stimulus-induced activity. Source reconstruction at trial level was performed independently for each mind state, and a t-test against the baseline (-0.25 to 0s relative to stimulus onset) was performed. Only statistically significant modulations of activity compared to the baseline (FDR corrected p-value<0.05, corrected for multiple comparisons across time, space and frequencies) are highlighted. While significant activations of visual streams (dorsal and ventral) were observable for both ON and MW conditions, starting from 200ms post-stimulus, this was not observed during MB trials.

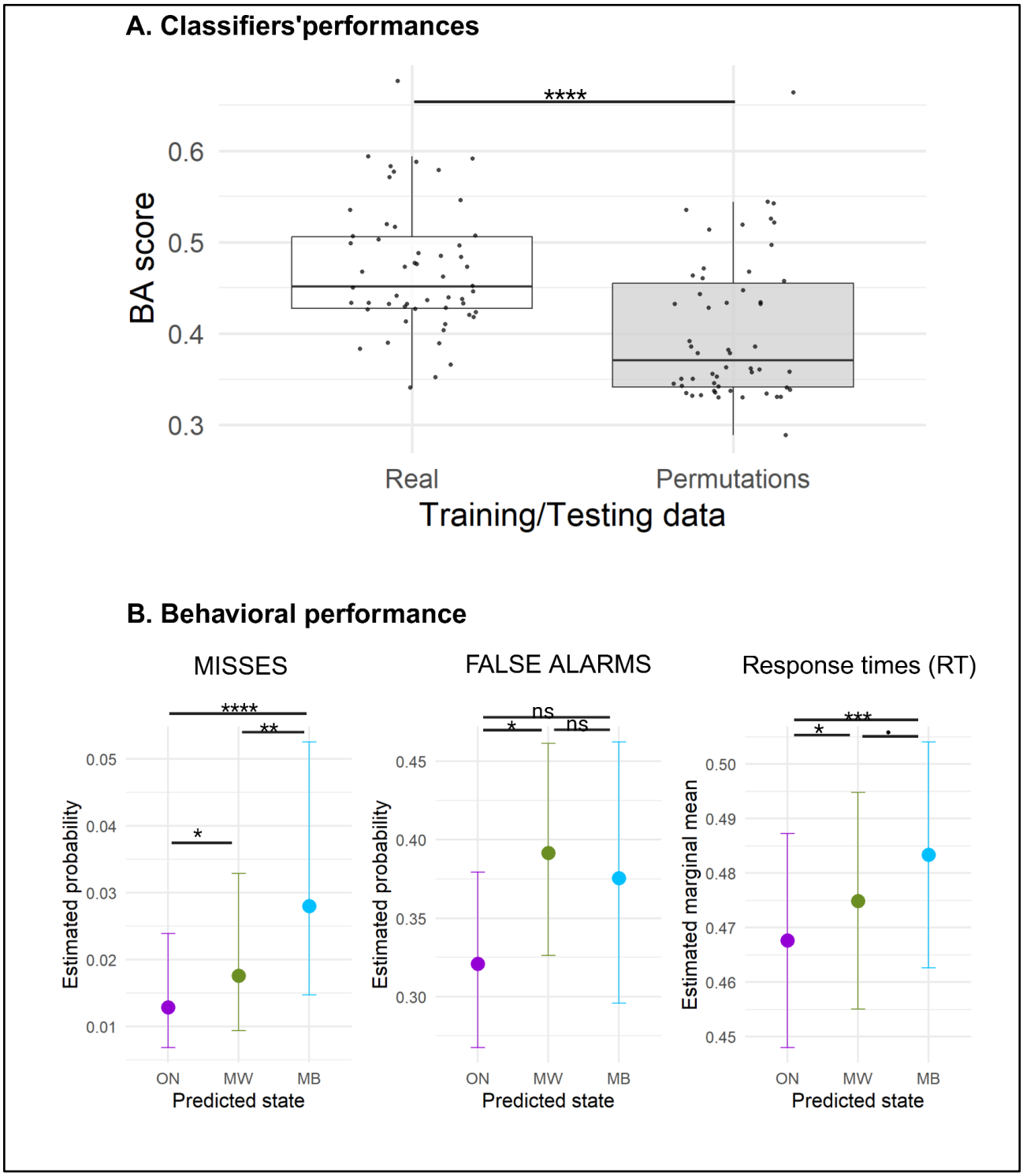

Figure 6: Trial-by-trial prediction of mind-state using a multivariate combination of neural markers. Panel A: Distribution of performances (balanced accuracy) of subject-level classifiers, both for true data and permuted data (mean score of 500 labels permutations). The classifier was trained and tested by cross-validation using labeled trials (<5 seconds before probe onsets). Spectral, complexity, connectivity, and ERP markers were used as raw features, followed by a dimensionality reduction by (non-linear) PCA. Only subjects presenting

with the 3 mind-states were included in this analysis. Panel B: Behavioral markers as a function of the predicted mind state in non-labeled trials (>5s before probe onsets). (Binomial) linear mixed models were computed with predicted mind-state as the main explanatory factor, and subject ID/dataset as random intercepts. Statistical bars represent pairwise statistical comparisons between states. We found very similar behavioral patterns for predicted trials as compared to reported (labeled) trials.

The detailed statistical results can be found in Table S6.
****: FDR corrected p-value<0.0001
***: FDR corrected p-value<0.001
**: FDR corrected p-value<0.01
*: FDR corrected p-value<0.05
▪ : FDR corrected p-value<0.1
n.s.: FDR corrected p-value>0.1

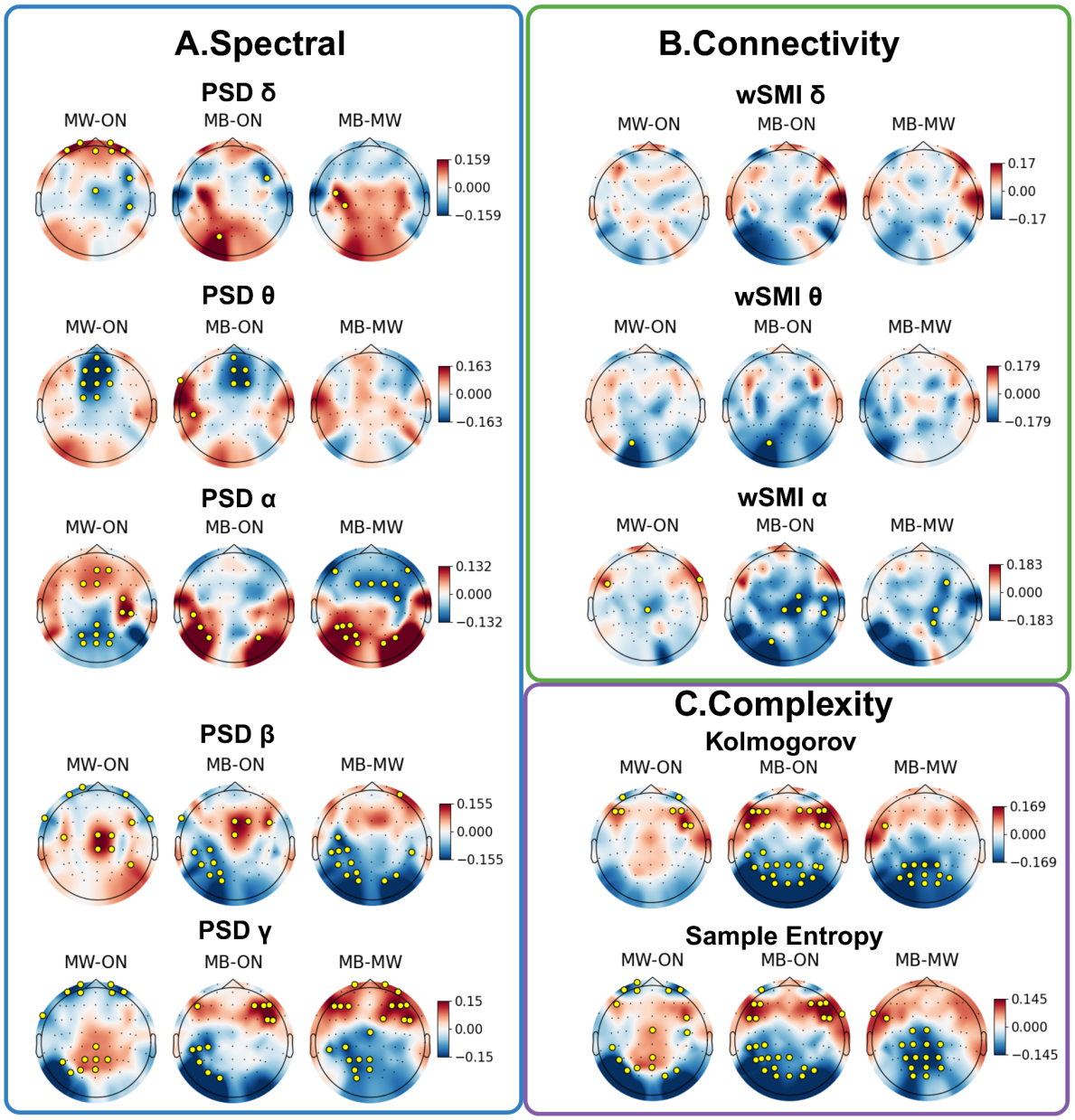

Figure S1: Modulation of EEG markers by mind-state corrected for vigilance modifications. Spectral (A), Connectivity (B) and Complexity (C) results. Each subplot represents the pairwise statistical contrast between two states (left: MW - ON; middle: MB - ON; right: MB - MW), at sensor level. Statistical models included the main effect of mind -state, electrode location and vigilance score (4-point scale, 1 = Extremely Sleepy, 4 = Extremely Alert), as well as the interactions mind-state/electrode location and vigilance score/electrode location. Subject ID and dataset were included as random intercepts. Model estimates for the contrast between states were computed for each electrode, and locations with statistically significant differences (FDR corrected p-value<0.05) are depicted with a golden circle. The observed results reproduced closely the results obtained with models not including vigilance score as a covariate (see main Figure 2).

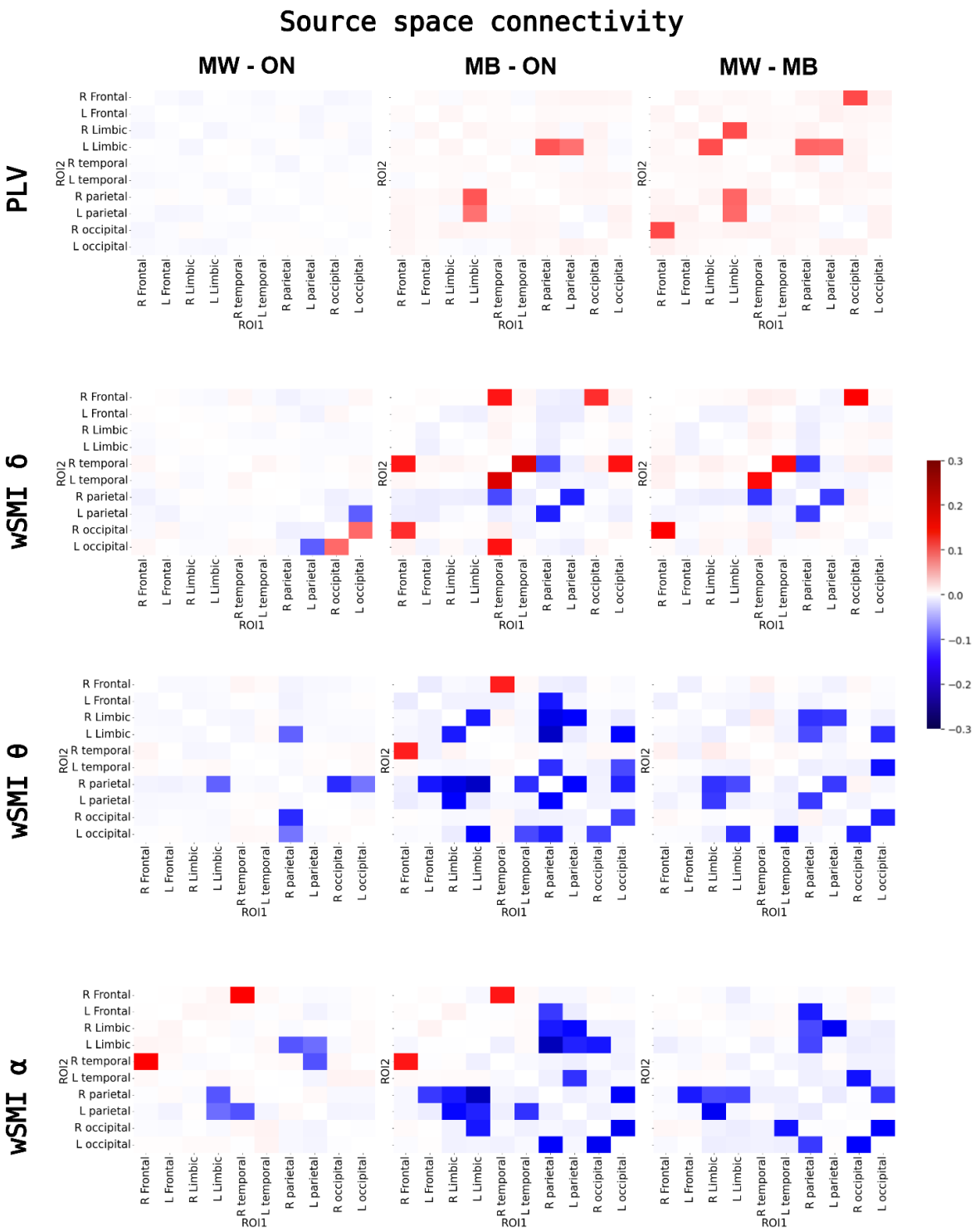

Figure S2: Modulation of source space connectivity by mind-state corrected for vigilance modifications. The PLV (top) and the wSMI in different frequency bands were computed at the source level. Each square-matrix represents the contrast in connectivity,

computed in source space, between two mind-states, for each pair of regions of interest (ROIs). Only significantly different connections (FDR corrected p-value<0.05) are highlighted, the other ones are masked. Statistical models included the main effect of mind -state, electrode location and vigilance score (4-point scale, 1 = Extremely Sleepy, 4 = Extremely Alert), as well as the interactions mind-state/electrode location and vigilance score/electrode location. Subject ID and dataset were included as random intercepts We observed a dissociation between the PLV and wSMI, with increased PLV (phase synchrony) and decreased wSMI (information sharing) between distant cortical areas, in particular in the theta and alpha bands, during MB, as compared to ON and MW. These results are similar to those obtained without including the vigilance score in the statistical models (see Figure 3).

δ: delta band; θ: theta band; α: alpha band
wSMI: weighted symbolic mutual information
PLV: Phase Locking Value
R: right; L: left

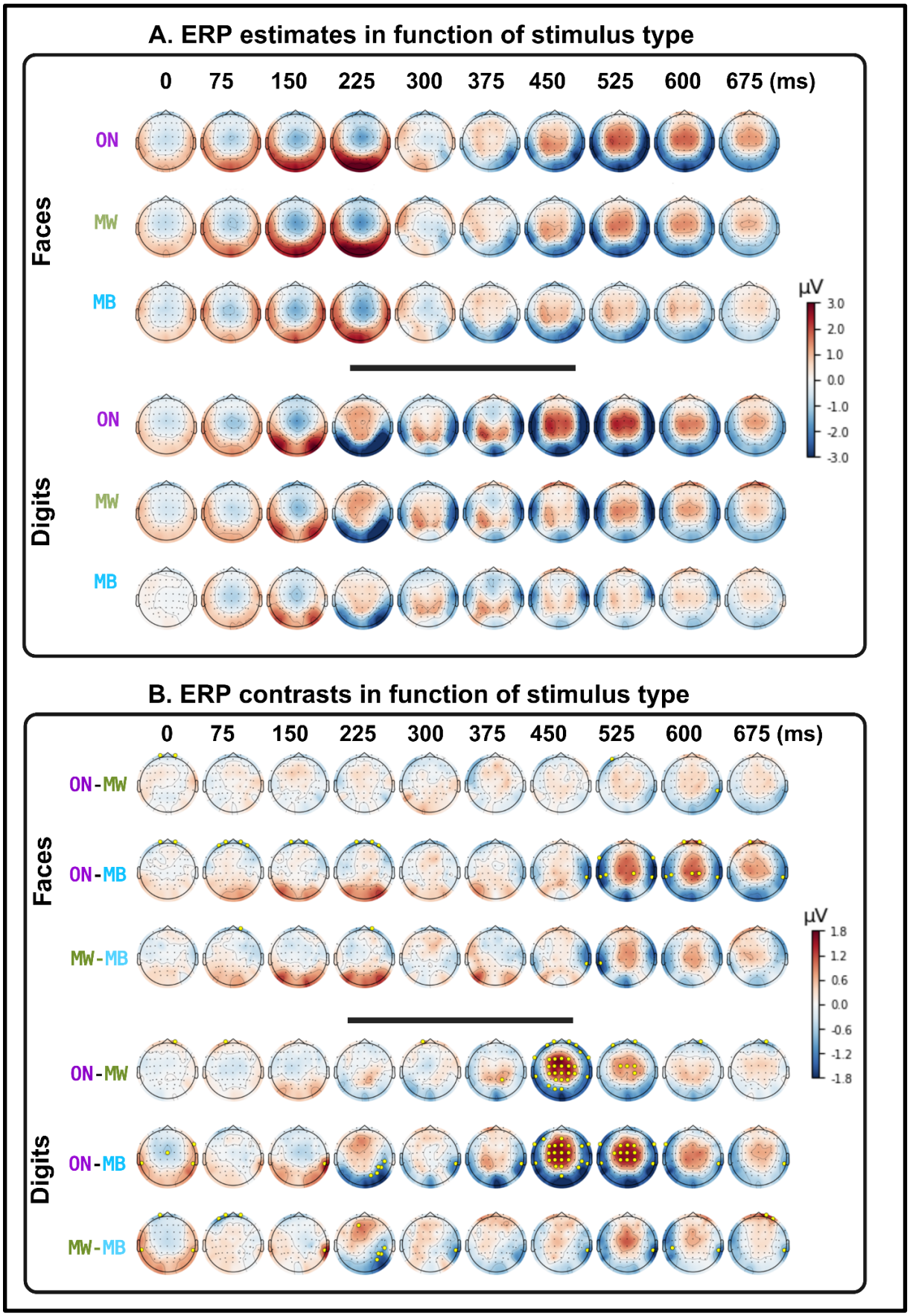
A. ERP estimates in function of stimulus type
0
75
150
225
300
375
450
525
600
675 (ms)
Faces
ON
MW
MB
Digits
ON
MW
MB
µV
3.0
2.0
1.0
0.0
-1.0
-2.0
-3.0
B. ERP contrasts in function of stimulus type
0
75
150
225
300
375
450
525
600
675 (ms)
Faces
ON-MW
ON-MB
MW-MB
Digits
ON-MW
ON-MB
MW-MB
µV
1.8
1.2
0.6
0.0
-0.6
-1.2
-1.8

Figure S3: ERP results independently for faces and digits. Panels A and B: Topographical scalp representation of the ERP estimates for each mind state (A) and ERP contrasts between mind-states (B), derived from the statistical model (single-trial multi-level analysis with mind-state, EEG channel and their interaction as main factors, and subject ID/dataset as random intercepts). Marked electrodes in panel B (golden circles) are the ones presenting a statistically significant difference between conditions (FDR corrected p-value<0.05). As seen in the figure, the analysis was conducted independently for faces and digits. ERPs ‘ profiles in function of the reported mind-state were consistent across stimuli types.

SUPPLEMENTARY RESULTS

TABLES

Mental state	FA (%)	Misses (%)	RTs (ms)
ON	24.5 ± 2.0	10.1 ± 0.9	471 ± 10
MW	46.1 ± 2.7	12.4 ± 1.1	465 ± 10
MB	39.9 ± 3.7	16.5 ± 1.6	480 ± 11

Behavioral measure	Main effect of mind state		Pairwise contrasts
	χ^2	***FDR corrected p-value***	
FA	χ^2 (2)=69.8	$8.3 * 10^{-15}$	<u>MW *vs* ON</u> : z-ratio=8.2, p-value= $5.0 * 10^{-15}$ <u>MB *vs* ON:</u> z-ratio=4.5, p-value= $2.5 * 10^{-5}$ <u>MB vs MW:</u> z-ratio=-1.6 p-value=0.12
Misses	χ^2 (2)=64.0	$7.6 * 10^{-14}$	<u>MW *vs* ON</u> : z-ratio=3.9, p-value= $2.4 * 10^{-4}$ <u>MB *vs* ON:</u> z-ratio=8.0, p-value= $1.8 * 10^{-14}$ <u>MB vs MW:</u> z-ratio=4.6 p-value=$1.7 * 10^{-5}$

RT	F (2)=5.2	$9.4 * 10^{-3}$	<u>MW *vs* ON</u> : z-ratio=-1.67, p-value= 0.1 <u>MB *vs* ON:</u> z-ratio=2.1, p-value= 0.043 <u>MB vs MW:</u> z-ratio=3.2 p-value=$2.6 * 10^{-3}$

Table S1: Behavioral results in labeled trials. Results of the linear mixed models with mind-state as a main factor and subject ID/dataset as random intercepts, for false alarms (FA), misses and response times (RT). The table presents the model estimates for each mind-state (top) and the statistical contrasts (bottom). All p-values were corrected for multiple comparisons using an FDR procedure.

EEG metric	Mind -state		Channel location		Mind-state:Channel	
	F (2)	p-value	F (63)	p-value	F (126)	p -value
Kolmogorov	19.8	3.78E-09	356.7	0	6.3	1.5E-97
Sample Entropy	46.7	9.49E-21	747.3	0	9.6	2.5E-175
normalized PSD delta	5.9	0.003542	99.6	0	3.1	3.5E-28
normalized PSD theta	8.34	0.00031	503.1	0	9.3	4.0E-169
normalized PSD alpha	62.3	1.73E-27	1335.2	0	6.5	4.3E-101
normalized PSD beta	8.3	0.000318	235.9	0	7.0	1.6E-113
normalized PSD gamma	9.4	0.000109	1180.2	0	10.0	1.5E-186
wSMI delta	37.4	1.03E-16	50.6	0	0.9	0.7
wSMI theta	57.9	1.37E-25	51.8	0	1.0	0.4
wSMI alpha	77.5	4.74E-34	69.3	0	1.9	1.1E-08

Table S2: Neural markers results (sensor space). ANOVA tables of the statistical models computed for each neural marker in sensor space (linear mixed models with mind state, electrode location and their interaction as main factors, and subject ID/dataset as a random intercepts). P-values were corrected for multiple comparisons using an FDR procedure.

Connectivity metric	Mind-state		Connection		Mind-state:Connection	
	F (2)	p-value	F (44)	p-value	F (88)	p-value
wSMI alpha	32.9	8.52E-15	352.5	0	1.7	0.0001
wSMI theta	42.9	3.95E-19	213.3	0	1.1	0.2
wSMI delta	24.8	2.9E-11	203.8	0	1.2	0.1

Table S3: Source-level connectivity. ANOVA tables of the statistical models computed for each connectivity measure in source space (linear mixed models with mind state, connection ID and their interaction as main factors, and subject ID/dataset as random intercepts). P-values were corrected for multiple comparisons using an FDR procedure.

Time-window (-/+ 25ms)	Mind-state		Channel location		Mind-state:Channel location	
	F (2)	p-value	F (63)	p-value	F (126)	p-value
0 ms	0.3	0.8	48.9	0	1.9	5.3E-10
75 ms	0.5	0.7	83.2	0	1.9	8.0E-10
150 ms	0.3	0.8	138.9	0	1.5	0.0003
225 ms	0.2	0.9	32.0	0	1.8	3.1E-07
300 ms	0.2	0.9	34.5	0	1.1	0.4
375 ms	0.07	0.9	38.9	0	1.8	3.4E-08
450 ms	0.2	0.9	91.9	0	6.6	8.6E-103
525 ms	0.5	0.7	119.9	0	7.7	2.1E-130
600 ms	0.6	0.6	83.8	0	4.4	1.6E-55
675 ms	0.3	0.8	52.4	0	2.7	1.5E-21

Table S4 : Event related potentials (ERPs). ANOVA tables of the statistical models computed at each time window (linear mixed models with mind state, electrode location and their interaction as main factors, and subject ID/dataset as random intercepts). P-values were corrected for multiple comparisons using an FDR procedure.

	ON	MW	MB
Precision	0.598	0.498	0.278
Recall	0.631	0.516	0.309
F1-score	0.605	0.498	0.289

Table S5: Weighted-average performance of individual's classifiers (PCA/Random Forest classifier) for each mind-state. The metrics (precision, recall, f1-score) are computed as the weighted mean across subjects, where each subject's contribution is weighted by the number of trials (support) for the respective class.

Subject	MB			MW			ON			Balanced accuracy/permutation test		
	Pr	Re	F1	Pr	Re	F1	Pr	Re	F1	Observed	Perm mean	p-value
Monash 001	NA	NA	NA	0.562	0.551	0.557	0.745	0.753	0.749	0.6805	0.5035	0.0040
Monash 002	NA	NA	NA	0.316	0.200	0.245	0.913	0.951	0.931	0.7321	0.6503	0.0200
Monash 003	**0.403**	**0.475**	**0.436**	**0.200**	**0.162**	**0.179**	**0.299**	**0.277**	**0.287**	**0.3524**	**0.3301**	**0.6387**
Monash 004	**0.392**	**0.305**	**0.343**	**0.237**	**0.136**	**0.173**	**0.475**	**0.656**	**0.551**	**0.4325**	**0.3340**	**0.0080**
Monash 005	**0.075**	**0.167**	**0.103**	**0.218**	**0.449**	**0.294**	**0.700**	**0.295**	**0.415**	**0.4505**	**0.3451**	**0.1018**

Monash 006	NA	NA	NA	0.794	0.992	0.882	0.000	0.000	0.000	0.5943	0.5961	0.8563
Monash 007	**0.133**	**0.053**	**0.075**	**0.511**	**0.627**	**0.563**	**0.291**	**0.255**	**0.272**	**0.4134**	**0.3917**	**0.8822**
Monash 008	**0.115**	**0.111**	**0.113**	**0.486**	**0.493**	**0.490**	**0.427**	**0.424**	**0.426**	**0.4336**	**0.3583**	**0.1058**
Monash 009	**0.432**	**0.488**	**0.458**	**0.476**	**0.291**	**0.361**	**0.155**	**0.391**	**0.222**	**0.4272**	**0.3503**	**0.0259**
Monash 010	**0.244**	**0.270**	**0.256**	**0.450**	**0.386**	**0.415**	**0.426**	**0.433**	**0.430**	**0.4103**	**0.3322**	**0.0758**
Monash 011	NA	NA	NA	0.000	0.000	0.000	0.845	0.992	0.912	0.6955	0.6986	0.9082
Monash 012	**0.264**	**0.383**	**0.313**	**0.569**	**0.412**	**0.478**	**0.298**	**0.364**	**0.327**	**0.4037**	**0.3387**	**0.3353**
Monash 013	NA	NA	NA	NA	NA	NA	1.000	1.000	1.000	1.000	1.000	1.0
Monash 014	**0.000**	**0.000**	**0.000**	**0.174**	**0.043**	**0.069**	**0.634**	**0.899**	**0.744**	**0.5769**	**0.5442**	**0.2255**
Monash 015	**0.000**	**0.000**	**0.000**	**0.531**	**0.673**	**0.594**	**0.423**	**0.275**	**0.333**	**0.4281**	**0.3855**	**0.6327**
Monash 016	**0.232**	**0.333**	**0.274**	**0.429**	**0.368**	**0.396**	**0.282**	**0.296**	**0.289**	**0.3891**	**0.3428**	**0.4471**
Monash 017	**0.059**	**0.046**	**0.052**	**0.298**	**0.330**	**0.313**	**0.533**	**0.550**	**0.541**	**0.3408**	**0.3408**	**0.6248**
Monash 018	**0.000**	**0.000**	**0.000**	**0.678**	**0.775**	**0.723**	**0.100**	**0.070**	**0.083**	**0.4963**	**0.4604**	**0.6906**
Monash 019	**0.503**	**0.593**	**0.545**	**0.239**	**0.145**	**0.180**	**0.323**	**0.352**	**0.337**	**0.4368**	**0.3373**	**0.2076**
Monash 020	**0.000**	**0.000**	**0.000**	**0.135**	**0.086**	**0.105**	**0.757**	**0.864**	**0.807**	**0.4522**	**0.4338**	**0.4691**
Monash 021	**0.000**	**0.000**	**0.000**	**0.086**	**0.049**	**0.062**	**0.710**	**0.850**	**0.774**	**0.5463**	**0.5257**	**0.8204**

Monash 022	**0.000**	**0.000**	**0.000**	**0.547**	**0.611**	**0.577**	**0.552**	**0.540**	**0.546**	**0.5877**	**0.4632**	**0.2056**
Monash 023	**0.000**	**0.000**	**0.000**	**0.423**	**0.294**	**0.347**	**0.642**	**0.782**	**0.705**	**0.5031**	**0.4343**	**0.0878**
Monash 024	**0.000**	**0.000**	**0.000**	**0.359**	**0.137**	**0.199**	**0.540**	**0.859**	**0.663**	**0.3831**	**0.3305**	**0.0399**
Monash 025	NA	NA	NA	0.783	0.864	0.822	0.348	0.232	0.278	0.6912	0.5992	0.0259
Monash 026	**0.000**	**0.000**	**0.000**	**0.778**	**0.871**	**0.822**	**0.420**	**0.300**	**0.350**	**0.5712**	**0.5423**	**0.1677**
Paris 001	**0.211**	**0.154**	**0.178**	**0.521**	**0.656**	**0.580**	**0.393**	**0.276**	**0.324**	**0.4264**	**0.3355**	**0.0299**
Paris 002	**0.480**	**0.571**	**0.522**	**0.316**	**0.276**	**0.294**	**0.385**	**0.321**	**0.350**	**0.4377**	**0.3528**	**0.3154**
Paris 003	**0.389**	**0.323**	**0.353**	**0.637**	**0.745**	**0.687**	**0.148**	**0.085**	**0.108**	**0.4181**	**0.3615**	**0.1617**
Paris 004	**0.130**	**0.062**	**0.085**	**0.366**	**0.293**	**0.325**	**0.400**	**0.540**	**0.460**	**0.4414**	**0.3783**	**0.4511**
Paris 005	**0.358**	**0.375**	**0.366**	**0.463**	**0.452**	**0.458**	**0.398**	**0.398**	**0.398**	**0.4325**	**0.3374**	**0.0200**
Paris 006	**0.000**	**0.000**	**0.000**	**0.382**	**0.366**	**0.374**	**0.647**	**0.776**	**0.706**	**0.4394**	**0.3603**	**0.0479**
Paris 007	**0.000**	**0.000**	**0.000**	**0.520**	**0.552**	**0.536**	**0.700**	**0.684**	**0.692**	**0.5831**	**0.4713**	**0.0160**
Paris 008	**0.161**	**0.310**	**0.212**	**0.388**	**0.392**	**0.390**	**0.655**	**0.547**	**0.596**	**0.5069**	**0.3629**	**0.0020**
Paris 009	**0.309**	**0.630**	**0.415**	**0.312**	**0.164**	**0.215**	**0.721**	**0.613**	**0.663**	**0.4295**	**0.3346**	**0.0060**
Paris 010	**0.200**	**0.222**	**0.211**	**0.443**	**0.360**	**0.397**	**0.678**	**0.729**	**0.703**	**0.4759**	**0.3574**	**0.0020**
Paris 011	**0.000**	**0.000**	**0.000**	**0.125**	**0.017**	**0.030**	**0.629**	**0.914**	**0.745**	**0.5198**	**0.5191**	**0.7066**

Paris 012	**0.333**	**0.419**	**0.371**	**0.511**	**0.463**	**0.486**	**0.146**	**0.125**	**0.135**	**0.4235**	**0.3422**	**0.0958**
Paris 013	**0.461**	**0.519**	**0.488**	**0.000**	**0.000**	**0.000**	**0.611**	**0.725**	**0.663**	**0.4728**	**0.3503**	**0.0060**
Paris 014	**0.125**	**0.256**	**0.168**	**0.106**	**0.292**	**0.156**	**0.853**	**0.540**	**0.661**	**0.4463**	**0.3560**	**0.2774**
Paris 015	**0.000**	**0.000**	**0.000**	**0.351**	**0.283**	**0.313**	**0.837**	**0.884**	**0.860**	**0.5066**	**0.4472**	**0.0080**
Paris 016	**0.000**	**0.000**	**0.000**	**0.444**	**0.330**	**0.379**	**0.709**	**0.814**	**0.758**	**0.5167**	**0.4674**	**0.1198**
Paris 017	**0.354**	**0.347**	**0.350**	**0.118**	**0.095**	**0.105**	**0.589**	**0.628**	**0.608**	**0.4727**	**0.3302**	**0.0100**
Paris 018	**0.000**	**0.000**	**0.000**	**0.000**	**0.000**	**0.000**	**0.887**	**1.000**	**0.940**	**0.6767**	**0.6642**	**0.0359**
Paris 019	**0.000**	**0.000**	**0.000**	**0.000**	**0.000**	**0.000**	**0.746**	**0.946**	**0.834**	**0.4836**	**0.4969**	**1.0**
Paris 020	**0.000**	**0.000**	**0.000**	**0.250**	**0.328**	**0.284**	**0.783**	**0.731**	**0.756**	**0.5917**	**0.5353**	**0.1796**
Paris 021	NA	NA	NA	0.269	0.206	0.233	0.773	0.829	0.800	0.5267	0.4979	0.4311
Paris 022	**0.036**	**0.071**	**0.048**	**0.497**	**0.657**	**0.566**	**0.375**	**0.206**	**0.266**	**0.4624**	**0.3788**	**0.1876**
Paris 023	**0.000**	**0.000**	**0.000**	**0.000**	**0.000**	**0.000**	**0.600**	**0.907**	**0.722**	**0.4985**	**0.5135**	**0.7485**
Paris 024	**0.550**	**0.484**	**0.515**	**0.000**	**0.000**	**0.000**	**0.611**	**0.739**	**0.669**	**0.5353**	**0.4324**	**0.0160**
Paris 025	**0.447**	**0.273**	**0.339**	**0.350**	**0.500**	**0.412**	**0.377**	**0.460**	**0.414**	**0.4773**	**0.3320**	**0.0020**
Paris 026	**0.000**	**0.000**	**0.000**	**0.000**	**0.000**	**0.000**	**0.817**	**0.992**	**0.896**	**0.4333**	**0.4324**	**0.6567**
Paris 027	**0.000**	**0.000**	**0.000**	**0.579**	**0.596**	**0.587**	**0.627**	**0.631**	**0.629**	**0.5789**	**0.4578**	**0.0020**

Paris 028	**0.382**	**0.317**	**0.347**	**0.465**	**0.444**	**0.454**	**0.500**	**0.555**	**0.526**	**0.4328**	**0.3821**	**0.3253**
Paris 029	**0.000**	**0.000**	**0.000**	**0.590**	**0.727**	**0.651**	**0.432**	**0.312**	**0.363**	**0.4850**	**0.4429**	**0.0978**
Paris 030	**0.218**	**0.250**	**0.233**	**0.472**	**0.402**	**0.434**	**0.431**	**0.470**	**0.450**	**0.4202**	**0.2885**	**0.0020**
Paris 031	**0.091**	**0.042**	**0.057**	**0.270**	**0.233**	**0.250**	**0.687**	**0.768**	**0.725**	**0.4677**	**0.3857**	**0.0240**
Paris 032	NA	NA	NA	NA	NA	NA	1.000	1.000	1.000	1.000	1.000	1.0
Paris 033	**0.273**	**0.284**	**0.278**	**0.233**	**0.206**	**0.219**	**0.538**	**0.556**	**0.547**	**0.3660**	**0.3457**	**0.2176**
Paris 034	**0.000**	**0.000**	**0.000**	**0.462**	**0.362**	**0.406**	**0.621**	**0.728**	**0.670**	**0.5940**	**0.5215**	**0.1178**
Paris 035	**0.000**	**0.000**	**0.000**	**0.500**	**0.667**	**0.571**	**0.415**	**0.300**	**0.348**	**0.4877**	**0.4284**	**0.2475**
Paris 036	**0.222**	**0.229**	**0.225**	**0.315**	**0.299**	**0.307**	**0.560**	**0.574**	**0.567**	**0.3897**	**0.3309**	**0.0060**

Table S6: Detailed results of subject level classifiers. For each subject and each class, precision (Pr), recall (Re) and F-1 score are presented. For each subject, the observed balanced accuracy score, the mean balanced accuracy of the permutation test and the p-value of the permutation test are presented. Highlighted subjects (in bold) present with the 3 classes (3 mind states) and were included in the group analysis (Figure 6, n= 54/62)

Predicted Mental state	FA (%)	Misses (%)	RTs (ms)
ON	32.1 ± 2.9	1.3 ± 0.4	468 ± 10
MW	39.2 ± 3.5	1.8 ± 0.6	475 ± 10
MB	37.6 ± 4.2	2.8 ± 0.9	483 ± 11
Behavioral measure	**Main effect of mind state**		**Pairwise contrasts**
	χ²	***FDR corrected p-value***	
FA	χ^2 (2)=6.8	0.04	MW *vs* ON : z-ratio=2.5, p-value= 0.02 MB *vs* ON: z-ratio=1.5, p-value= 0.1 MB vs MW: z-ratio=-0.4, p-value=0.7
Misses	χ^2 (2)=31.5	$5.7 * 10^{-7}$	MW *vs* ON : z-ratio=2.4, p-value= 0.02 MB *vs* ON: z-ratio=5.6, p-value=$9.6 * 10^{-8}$ MB vs MW: z-ratio=3.3, p-value=0.002
RT	F (2)=7.4	$1.4 * 10^{-3}$	MW *vs* ON : z-ratio=2.3, p-value= 0.03 MB *vs* ON: z-ratio=3.6, p-value= $7.5 * 10^{-4}$ MB vs MW: z-ratio=1.8 p-value=0.08

Table S7: Behavioral results in non-labeled trials in function of the predicted mind-state. Results of the linear mixed models with predicted mind-state as a main factor and subject ID/dataset as random intercepts, for false alarms (FA), misses and response times (RT). The table presents the model estimates for each mind -state (top) and the statistical contrasts (bottom). P-values were corrected for multiple comparisons using an FDR procedure.